Water Mass Formation in an Isopycnal Model of the North Pacific

CAROL LADD AND LUANNE THOMPSON

School of Oceanography, University of Washington, Seattle, Washington

(Manuscript received 8 February 2000, in final form 8 August 2000)

ABSTRACT

An isopycnal model coupled with a mixed layer model is used to study transformation and formation rates in the North Pacific. When annual formation rates are averaged over the entire North Pacific, a large peak in water mass formation is found at a density of approximately $\sigma_\theta = 26$ kg m^{-3}. This peak in formation rate corresponds to the formation of North Pacific Central Mode Water (CMW) in the model. No corresponding peaks in formation rate are found at the densities of Subtropical Mode Water (STMW; $\sigma_\theta \sim 25.4$ kg m^{-3}) or Eastern Subtropical Mode Water (ESMW; $\sigma_\theta \sim 24$–25.4 kg m^{-3}) when averaged over the entire model basin. However, when calculated locally, enhanced formation rates are found at the densities of these mode water masses.

The formation of each of the three types of North Pacific mode water in the model occurs because of different circumstances. As expected, STMW formation is dependent on the strong cooling and resultant deep mixed layers over the Kuroshio Current region. However, formation rates in the STMW formation region (west of the date line) imply that most of the thickness maximum formed there each winter is subsequently reentrained into the mixed layer during the next winter where it is further cooled, preconditioning it to become denser varieties of STMW farther east. Similarly, preconditioning west of the formation region is important in CMW formation. Only 33% of the STMW escapes reentrainment the next winter. The STMW signature (minimum in vertical stratification) remains in the region in the next winter owing to a tight recirculation that carries the mode water south before the mixed layer deepens again the next winter. The renewal times calculated from the model are 1.5–5.5 yr for STMW and approximately 10–14 yr for CMW.

The ESMW formation is due to a band of weak positive formation combined with a wide layer outcrop. The only region where forcing by the atmosphere can directly influence an isopycnal layer is where the isopycnal layer outcrops into the mixed layer. The wide layer outcrop at ESMW densities (~30°N, 140°W) is at least partially due to weak summer heating in the southeastern part of the formation region. Only 13% of the ESMW volume escapes reentrainment by the mixed layer in the succeeding year contributing to a renewal time of only 1–2 yr.

1. Introduction

Much recent attention has been given to thermocline ventilation in the subtropical gyres of the North Atlantic and the North Pacific. When mixed layer water is detrained into the thermocline, it brings with it properties (such as temperature, salinity, potential vorticity, chemical tracer concentrations) formed through interaction with the atmosphere. If this mixed layer water subducts into or ''ventilates'' the *permanent* thermocline, those properties are insulated from further interaction with the atmosphere, thus modifying water properties and circulation patterns in the permanent thermocline.

The transformation rate is a quantitative measure of the influence of air–sea interactions on the thermocline. By combining heat and volume budgets for an isothermal layer, Walin (1982) derived relations between surface heat fluxes and water mass formation in the absence of diffusion. Surface buoyancy fluxes change the density of the surface water causing isopycnal outcrops to move north and south over the annual cycle. In a reference frame that follows the isopycnal surfaces, *transformation* (water is *transformed* from one density to another) is defined as a diapycnal volume flux across potential density surfaces due to buoyancy fluxes. Assuming the spacing of isopycnal outcrops is unchanged from year to year, then convergences in transformation lead to *formation* of subsurface water.

Speer and Tziperman (1992), Tziperman and Speer (1994), and Speer et al. (1995, 1997), use various buoyancy flux datasets to estimate formation rates in the North Atlantic, the Mediterranean, the World Ocean, and the Southern Ocean, respectively. Nurser et al. (1999) and Marsh et al. (2000) use an isopycnal model to estimate formation rates (including the effects of entrainment and diffusion) in the North Atlantic and the Southern Ocean, respectively. Speer and Tziperman

Corresponding author address: Dr. Carol Ladd, NOAA/PMEL, 7600 Sandpoint Way, Seattle, WA 98115-6349.
E-mail: carol.ladd@noaa.gov

(1992) use three different climatological datasets (Budyko 1956; Isemer and Hasse 1987; Bunker 1976) to calculate transformation rates. They find a peak in transformation rate in the North Atlantic at a density of $\sigma_\theta = 26.3$ kg m^{-3} for all three datasets but the magnitude of the peak varies from ~30 Sv (Isemer and Hasse; Bunker) to over 40 Sv (Budyko) (Sv $\equiv 10^6$ m^3 s^{-1}). Using the Esbensen and Kushnir (1981) climatology, Nurser et al. (1999) find a maximum transformation rate of only 19 Sv at $\sigma_\theta = 26.5$ kg m^{-3} for the same region of the North Atlantic. With the exception of the Nurser et al. (1999) and Marsh et al. (2000) studies, formation rates have generally been calculated from surface buoyancy fluxes alone (excluding the effects of mixing). By using a model, we can analyze the effects of mixing on formation rates.

In addition, formation rates as a function of density have traditionally been calculated as an integral quantity over an entire isopycnal outcrop region. By examining the geographical distribution of formation on any isopycnal layer, we can relate formation rates to mode water formation, a more localized process. Because mode water formation occurs in localized regions where formation rates are large, mode water formation may be an important method of transmitting the effects of atmospheric forcing to the subsurface ocean.

Worthington (1959) first recognized the importance of mode water with his study of 18° Water in the subtropical North Atlantic. In the North Pacific, three kinds of mode waters have been identified: North Pacific Subtropical Mode Water (STMW) in the western North Pacific (Masuzawa 1969), Central Mode Water (CMW) in the central North Pacific (Nakamura 1996; Suga et al. 1997), and Eastern Subtropical Mode Water (ESMW) in the eastern North Pacific (Hautala and Roemmich 1998). The relative importance of atmospheric forcing and ocean stratification in the formation of these mode waters remains unclear.

The North Pacific STMW is the most intensively studied mode water in the North Pacific. Worthington (1959), in his study of the North Atlantic 18° Water, first noted the existence of a thermostad at 16.5°C in the North Pacific. Masuzawa (1969, 1972) described distributions of this North Pacific variety of STMW. Nakamura (1996) estimated the average density of STMW to be $\sigma_\theta = 25.42$ kg m^{-3}. The formation region for STMW is a region of strong winter cooling (>400 W m^{-2}) (da Silva et al. 1994) and deep winter mixed layers (>200 m).

The North Pacific CMW has only recently been identified (Nakamura 1996; Suga et al. 1997). The CMW pycnostad is identified by low potential vorticity (PV) on the $\sigma_\theta = 26.2$ kg m^{-3} isopycnal surface in the central subtropical gyre (see Fig. 4 in Talley 1988). By analyzing *T–S* diagrams limited to parcels of water with potential vorticity less than 1.5×10^{-10} m^{-1} s^{-1}, Nakamura (1996) estimates a characteristic σ_θ range of 26.0–26.5 kg m^{-3} for CMW. The formation region for CMW is to the east of the STMW formation region and it has been suggested that preconditioning supplied by the STMW formation allows the CMW to form (Ladd and Thompson 2000). Heat losses in the CMW formation region are weaker than in the STMW formation region (>175 W m^{-2}) (da Silva et al. 1994) but mixed layer depths are as deep or deeper than in the STMW formation region (>240 m) (Ladd and Thompson 2000).

Talley (1988) identifies a lateral minimum in potential vorticity in the eastern Pacific centered at approximately 30°N, 140°W. She points out that this minimum lies under a region of maximum Ekman downwelling. Hautala and Roemmich (1998) study this potential vorticity minimum in more detail and identify it as Eastern Subtropical Mode Water (σ_θ range of 24.0–25.4 kg m^{-3}), a mode water distinct from both the STMW and the CMW. From climatology data, Ladd and Thompson (2000, their Fig. 4) find a σ_θ range of 25.0–25.25 kg m^{-3} for ESMW, slightly lighter than the STMW density range. Hautala and Roemmich note that formation mechanisms for ESMW are unclear because winter cooling is fairly weak in the ESMW formation region (130 W m^{-2} at 30°N, 140°W) (da Silva et al. 1994). Ladd and Thompson (2000) find that weak summer heating in this region results in weak stratification at the beginning of the cooling season, allowing mixed layers to deepen more than they would otherwise, contributing to the formation of ESMW.

In this study, following the work of Nurser et al. (1999) in the North Atlantic and Marsh et al. (2000) in the Southern Ocean, formation rates are calculated for the North Pacific using an isopycnal general circulation model. The model allows us to relate formation rates for specific isopycnal layers to the formation of mode waters and to analyze the relative contributions of atmospheric forcing and ocean stratification. In addition, we analyze the circulation and subsequent destruction of the mode waters after formation. The remainder of this paper is organized as follows: section 2 provides a description of the isopycnal model and sensitivity studies. Section 3 provides derivations of the transformation and formation rates that are discussed in sections 4 and 5 respectively. Section 6 relates regional formation rates to mode water formation and discusses mode water circulation. Section 7 provides discussion and conclusions.

2. Isopycnal model

The model used for this study is the Hallberg isopycnal model (Hallberg 1995; Thompson et al. 2000, manuscript submitted to *J. Phys. Oceanogr.*) It is configured with 15 layers in the vertical including a Kraus–Turner (1967) bulk mixed layer, a variable density buffer layer to handle mixed layer detrainment, and 13 isopycnal layers. The layer densities were chosen in an attempt to distinguish the various mode waters (Subtropical, Central, and Eastern Subtropical Mode Waters) observed in the North Pacific (Table 1). The model do-

TABLE 1. Density of model layers and mode water masses.

Layer index	Density (σ_θ)	Water mass
1 (mixed layer)	Variable	
2 (buffer layer)	Variable	
3	22.5	
4	23.5	
5	24.25	
6	24.75	ESMW
7	25.125	STMW, ESMW
8	25.375	STMW, ESMW
9	25.625	STMW
10	25.875	CMW
11	26.125	CMW
12	26.375	CMW
13	26.75	
14	27.25	
15	27.75	

main (20°S–60°N, 126°E–76°W) covers the entire North Pacific with realistic topography and coastline and a horizontal resolution of 2 degrees.

The buffer layer is used to avoid static instability during mixed layer detrainment. When the variable density mixed layer detrains water, the water will typically have a density that is not equal to any of the isopycnal layer densities. Thus, in order to conserve buoyancy, the water must be apportioned between two isopycnal layers (one lighter than the detrained water and one denser). If the lighter isopycnal layer is less dense than the current mixed layer density above it, then putting mass into the layer will cause static instability. Instead, the detrained water is retained in the buffer layer at the density at which it was detrained from the mixed layer. Once the mixed layer has become sufficiently light that apportioning the detrained water into isopycnal layers will not cause instabilities, the buffer layer detrains into the isopycnal layers.

a. Initialization and forcing

Mixed layer densities and isopycnal layer thicknesses are initialized with sea surface densities and layer thicknesses calculated from climatological September temperature and salinity values (Levitus et al. 1994; Levitus and Boyer 1994). At all open boundaries (along 20°S, the Indonesian Throughflow, and the Bering Sea), the layer thicknesses are continually relaxed to monthly climatological values with a relaxation timescale of 15 days. These sponge layers allow for water mass sources at the open boundaries.

The model is forced at the surface with daily linear interpolations of monthly mean climatological heat and freshwater fluxes (converted to density fluxes) and surface winds from the *Atlas of Surface Marine Data 1994* (da Silva et al. 1994, hereafter *ASMD*). In addition, to keep surface density values from drifting too far from reality, it is necessary to relax the mixed layer density to daily interpolations of monthly mean climatological surface density (Levitus et al. 1994; Levitus and Boyer 1994). The density flux at the surface is then

$$f = -\frac{\alpha Q}{C_p} + \frac{h}{\lambda}(\rho_{\text{obs}} - \rho_{\text{model}}) + \beta S(E - P), \quad (1)$$

where Q is the net heat flux from the atmosphere to the ocean (the sum of radiative, latent, and sensible fluxes) from the *ASMD*, α is the thermal expansion coefficient (monthly and latitudinally varying), C_p is the specific heat, h is an average mixed layer depth (taken to be 100 m), λ is a relaxation timescale (35 days), β is the haline contraction coefficient (0.775 kg m^{-3} psu^{-1}), S is surface salinity (35 psu), and $E - P$ is evaporation minus precipitation from the *ASMD*.

b. Diapycnal mass fluxes

Three primary processes contribute to mass fluxes between layers and thus to transformation rates (see section 3 for derivations): entrainment into the mixed layer due to convection and the turbulent kinetic energy supplied by wind mixing and turbulent buoyancy fluxes, detrainment from the mixed layer due to mixed layer warming and shoaling, and diapycnal diffusion between layers. The mixed layer formulation is described in detail by Thompson et al.

During periods when f is positive (i.e., during cooling: $Q < 0$), the mixed layer gets steadily denser. Whenever the mixed layer gets denser than the next heavier layer, that layer is entrained into the mixed layer, modifying the mixed layer density and conserving buoyancy. This results in a mass flux from the isopycnal layer (or the buffer layer) to the mixed layer.

During periods when f is negative (i.e., during warming), the mixed layer shoals to the Monin–Obukhov depth, the depth at which wind-generated turbulent kinetic energy balances the work required to mix the surface buoyancy forcing throughout the mixed layer depth. The remainder of the mixed layer is detrained into the buffer layer until it can be partitioned into isopycnal layers (conserving buoyancy) without causing static instability. This detrainment results in a mass flux from the mixed layer to the buffer layer (and, eventually, from the buffer layer to isopycnal layers).

Third, explicit diapycnal diffusion (between layers) is active in the model with a coefficient of $\kappa_d = 1 \times 10^{-5}$ m^2 s^{-1}, as suggested by tracer release experiments in the open ocean interior (Ledwell et al. 1993). Diapycnal diffusion results in mass fluxes between isopycnal layers. Although density varies laterally in the mixed layer and the buffer layer, the model has no explicit diapycnal diffusion (laterally) within the mixed layer or the buffer layer. Nurser et al. (1999) evaluate mixing processes in the North Atlantic. They find that lateral mixing in the mixed layer is fairly small relative to entrainment and interior diffusion between isopycnal layers especially in regions where the mixed layer is shallow. Because the mixed layers are relatively shallow

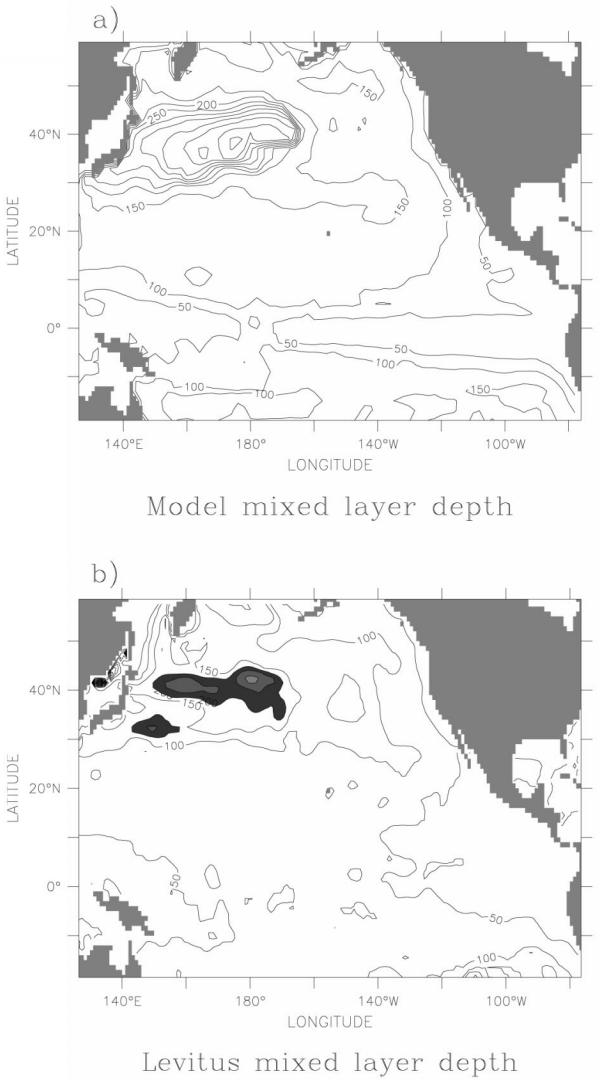

FIG. 1. Maximum mixed layer depth (contour interval: 50 m) for (a) model year 51 and (b) calculated from Levitus climatology with mixed layer depth defined as the depth at which σ_θ is 0.125 kg m^{-3} different from the sea surface. The two shaded regions denote local maxima in mixed layer depth corresponding to the STMW and the CMW formation regions.

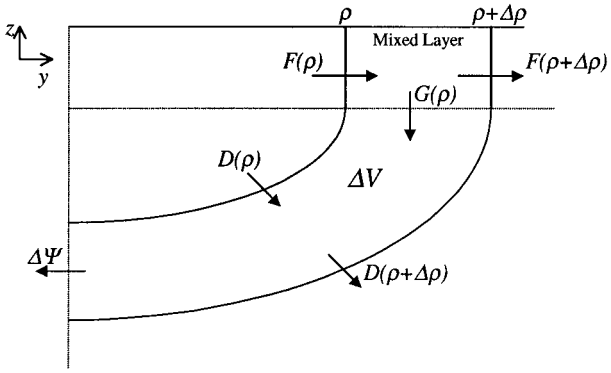

FIG. 2. Schematic vertical section of the mixed layer and an isopycnal layer: $F(\rho)$ is the volume flux across an isopycnal outcrop from Eq. (3) and G is the volume flux of fluid into the subsurface isopycnal layer from the mixed layer. Note that G includes both entrained and detrained fluid, and D is the volume flux between isopycnal layers due to diapycnal diffusion.

in the North Pacific as compared to the Atlantic, we expect that lateral diffusion in the mixed layer should be relatively unimportant.

c. Mixed layer depths: Sensitivity analysis

The annual maximum mixed layer depth calculated by the model exhibits deep mixed layers in a zonally elongated region along approximately 40°N and shallower mixed layer depths along the eastern and southern branches of the subtropical gyre, as well as along the equator. Given the limited horizontal resolution of the model, this pattern closely matches the maximum mixed layer depth calculated from climatological temperature and salinity data (Levitus et al. 1994; Levitus and Boyer 1994) (Fig. 1). However, the mixed layer depths calculated in the model are deeper than those calculated from climatology, especially in the region of deep mixed layers at approximately 40°N. This discrepancy in mixed layer depths is due to a combination of factors.

First, the limited vertical resolution of the model leads to deeper mixed layers because, when the mixed layer gets denser than an isopycnal layer, the mixed layer entrains the entire layer. In the real ocean, the depth of entrainment would be limited by continuous stratification. In addition, due to the heavy spatial and temporal smoothing in the Levitus climatology, maxima in mixed layer depth calculated from the climatology may be underestimated.

Second, due to the limited horizontal resolution, the Kuroshio tends to overshoot its separation from the western boundary. This leads to warm water flowing too far north. The relaxation density flux tries to counter the anomalously light sea surface density in this region, leading to large winter cooling over the model Kuroshio Extension. Another impact of the limited horizontal resolution is that the model mixed layer depth pattern is too broad. In the observations, a region of shallower mixed layer associated with the Kuroshio Extension separates two regions of deep mixed layers (denoted by shading in Fig. 1b). The model does not capture this structure. This is discussed further in section 5.

Third, the *ASMD* used to force the model may be inaccurate. Heat flux climatologies such as the *ASMD* can be expected to have errors on the order of 20 W m^{-2} (D. E. Harrison 1998, personal communication) and $E - P$ is even more uncertain. In addition, the *ASMD* wind stress climatology is based on the Comprehensive Ocean–Atmosphere Data Set and can be expected to have fairly large errors over the Sea of Okhotsk and other far northern regions due to a lack of observations.

Finally, the combination of limited resolution and in-

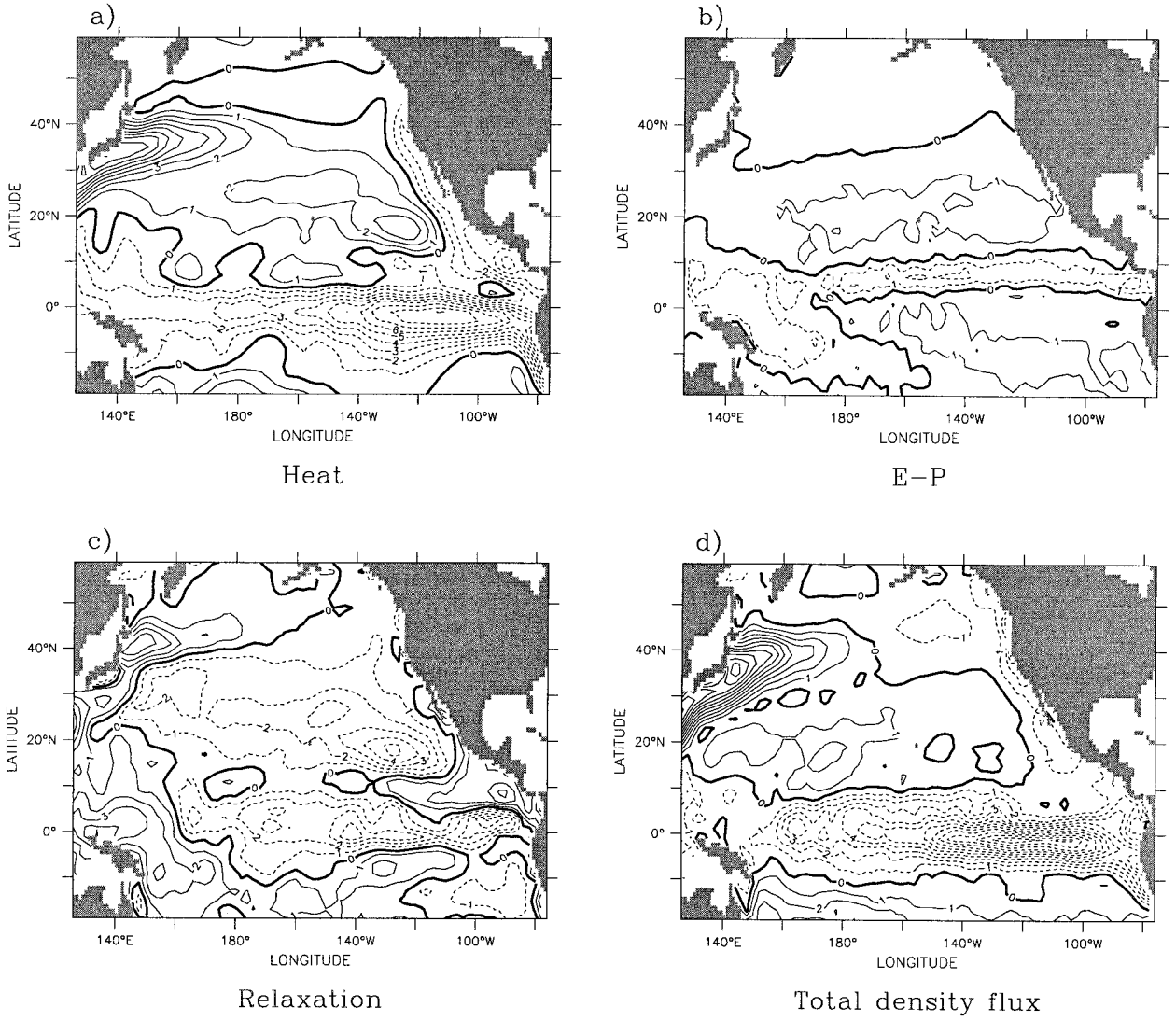

FIG. 3. Annual mean density flux in model year 51 (contour interval: 1.0×10^6 kg s^{-1} m^{-2}) (a) due to heat fluxes, (b) due to freshwater fluxes, (c) due to relaxation, and (d) total.

adequate forcing fields results in inaccurately modeled formation of North Pacific Intermediate Water (NPIW) resulting in an inaccurate vertical structure. To try to simulate a more realistic NPIW volume in the absence of realistic NPIW formation, a test run was undertaken in which the layer thicknesses in the Sea of Okhotsk (where NPIW is believed to be formed) were continually relaxed to wintertime climatological values. As expected, this model run improved the vertical structure. However, except in some details, our analysis and conclusions were essentially the same whether we analyzed the original model run or the model run with relaxation in the Sea of Okhotsk. That our conclusions remain unchanged suggests that they are fairly robust to change in NPIW ventilation, although further studies on the influence of NPIW formation are warranted.

In addition to the test run mentioned above (relaxation in the Sea of Okhotsk), many other test runs with differing forcing fields and/or relaxation regions were undertaken. Changing the heat fluxes and relaxation regions used to force the model had very little effect on the model results, suggesting that deficiencies in the model formulation are more fundamental than deficiencies in forcing fields. Insufficient resolution, both horizontally and vertically, is probably the most important. However, without drastically increasing our computer power, or the length of the model runs, it is difficult to increase the model resolution much more. Mixed layers that are too deep in the western Pacific compared with observations and a Kuroshio Current that overshoots its separation from the boundary imply that our results for the western part of the basin, particularly the STMW, are probably less robust than for the central and eastern part of the basin. However, we feel that the model can

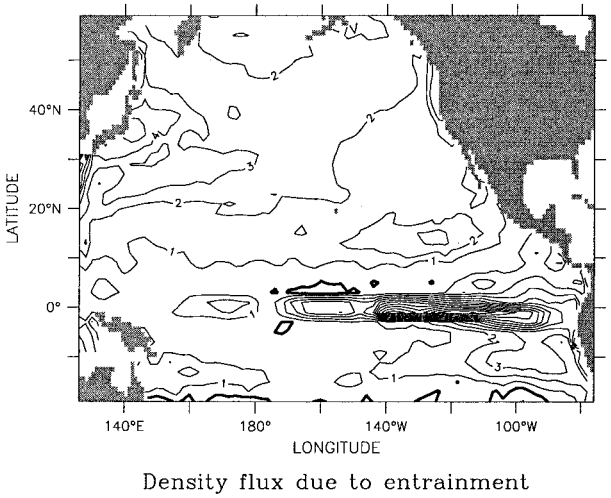

FIG. 4. Change in mixed layer density due to entrainment from below averaged over model year 51 (10^6 kg s^{-1} m^{-2}).

provide insight into the formation of mode waters in the North Pacific and their circulation after formation.

At the end of a 50 year spinup run, the model circulation, mixed layer densities, and isopycnal layer thicknesses do not change much from year to year. Results presented in this study are from year 51 of the original model run.

3. Derivations

By combining heat and volume budgets for an isothermal layer, Walin (1982) derived relations between surface heat fluxes and water mass formation in the absence of diffusion and mixing. Here, we modify Walin's relations (in terms of potential density) to correspond to an isopycnal model coupled with an explicit mixed layer. For this derivation, and throughout the rest of the paper, we will consider the buffer layer to be part of the mixed layer. We will consider the following geometry: an isopycnal layer of water with potential density between ρ and $\rho + \Delta\rho$ and a mixed layer with spatially varying potential density in a limited domain (Fig. 2). The only difference between the following derivations and those of Nurser et al. (1999) is that we treat the mixed layer separately. We define mode water as thick layers of nearly homogenous water that are *isolated from interaction with the atmosphere.* Thus, water is not considered mode water until it has been detrained from the mixed layer. Treating the mixed layer separately allows us to isolate the formation of mode water.

a. Density and volume budgets of the mixed layer

In the model, the only layers in which density can change are the mixed layer and buffer layer. As discussed above, mixed layer density is affected by surface

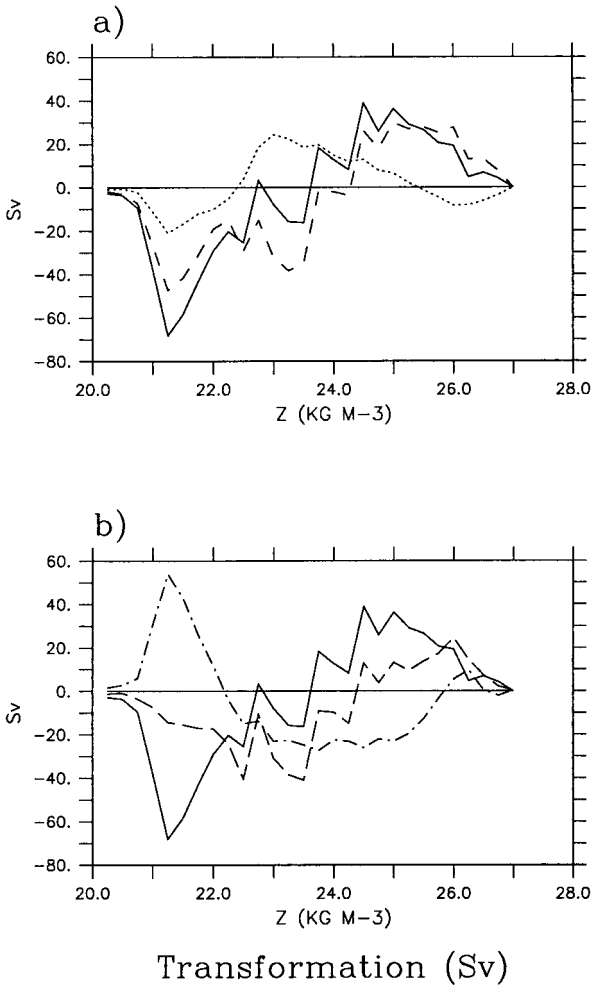

FIG. 5. Annual mean transformation (a) due to heat fluxes (dash), due to $E - P$ (dot), and total climatological (solid) and (b) due to relaxation (dash–dot), climatological (solid), and total relaxation + climatological (dash).

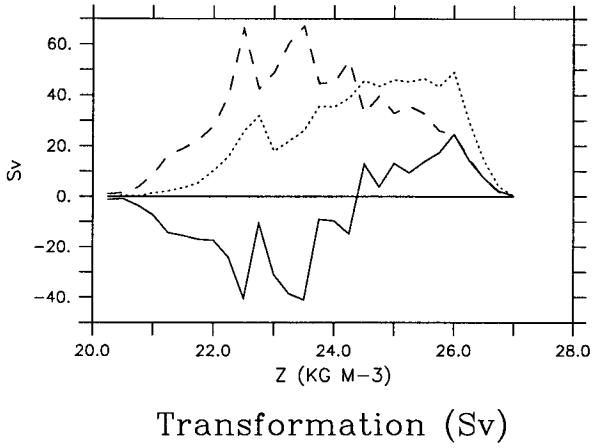

FIG. 6. Annual mean transformation due to $E - P$, heat fluxes, and relaxation (solid); due to entrainment into mixed layer from below (dash); and due to $E - P$, heat fluxes, relaxation, and entrainment (dot).

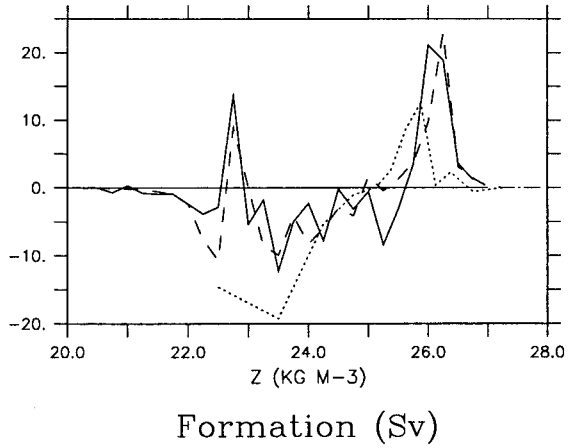

FIG. 7. Formation rate due to mixed layer density fluxes [$F(\rho) - F(\rho + \Delta\rho)$ solid], flux out of buffer layer ($G(\rho)$ dash), and flux into isopycnal layers directly from buffer layer (dot).

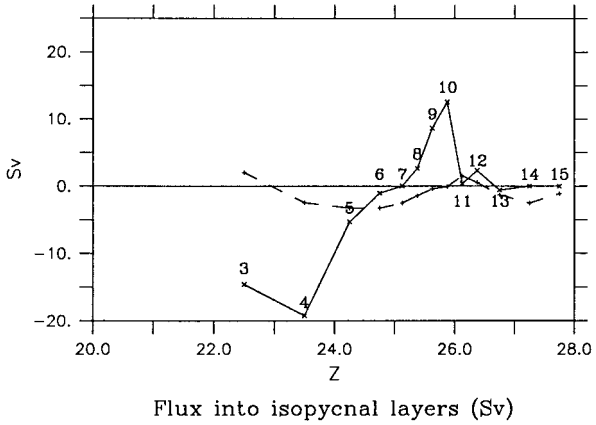

FIG. 8. Flux into isopycnal layers directly from buffer layer [$G(\rho)$: solid) and flux into isopycnal layers including diapycnal diffusive fluxes between layers [from Eq. (8): dash]. The numbers represent the layer indices.

density fluxes (consisting of heat fluxes, freshwater fluxes, and relaxation fluxes) and by entrainment of isopycnal layer water from below due to convective adjustment and wind mixing:

$$\frac{D\rho_{\mathrm{ML}}}{Dt} = \frac{f}{h_{\mathrm{ML}}} + \frac{w_{\mathrm{entr}}(\rho_k - \rho_{\mathrm{ML}})}{h_{\mathrm{ML}}}, \tag{2}$$

where D/Dt is the material derivative, f is the surface density flux from (1), w_{entr} is the flux of subsurface fluid into the mixed layer, ρ_k is the density of the fluid being entrained, and h_{ML} is the depth of the mixed layer. When the mixed layer density changes, the isopycnal outcrops in the mixed layer move (generally north–south). Now we change our reference frame to follow the isopycnal outcrops. Instead of thinking of outcrops moving through the fluid, we can think of fluid moving across the outcrops. The volume flux across an isopycnal outcrop is

$$F(\rho) = \lim_{\Delta\rho \to 0} \frac{1}{\Delta\rho} \iint_{\text{outcrop}} [f + w_{\mathrm{entr}}(\rho_k - \rho_{\mathrm{ML}})]\, dA. \tag{3}$$

We will call $F(\rho)$ the transformation rate following Speer and Tziperman (1992). Note that Speer and Tziperman defined $F(\rho)$ as transformation due to air–sea fluxes only and neglected the density flux due to entrainment.

When averaged over a year, some density ranges lose buoyancy while others gain buoyancy resulting in convergences and divergences in flux across isopycnal outcrops. If we assume isopycnal outcrop spacing and mixed layer depth do not change from year to year, then the mixed layer volume budget implies that convergences result in downward flux into the subsurface isopycnal layers:

$$F(\rho) - F(\rho + \Delta\rho) = \iint_{\text{outcrop}} (w_{\mathrm{detr}} - w_{\mathrm{entr}})\, dA = G(\rho), \tag{4}$$

where $G(\rho)$ is defined as the volume flux of fluid from the mixed layer into the isopycnal layer (including mixed layer entrainment and detrainment).

b. Volume budget of an isopycnal layer

Let ΔV be the volume of fluid in the isopycnal layer (not including mixed layer fluid), $\Delta\Psi$ be the volume flux of fluid with density between ρ and $\rho + \Delta\rho$ out of the domain, and $D(\rho)$ be the diffusive diapycnal flux of fluid across the ρ isopycnal surface. Note that in the isopycnal model framework, diapycnal diffusion is pa-

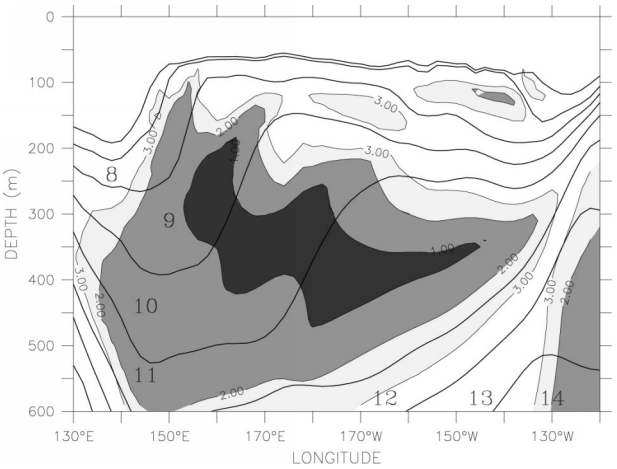

FIG. 9. Annual mean section along 29°N showing potential vorticity (shaded; contour interval, 1×10^{-10} m^{-1} s^{-1}; contours larger than 3×10^{-10} m^{-1} s^{-1} not displayed) and layer configuration (numbers 8–14 indicate layer indices).

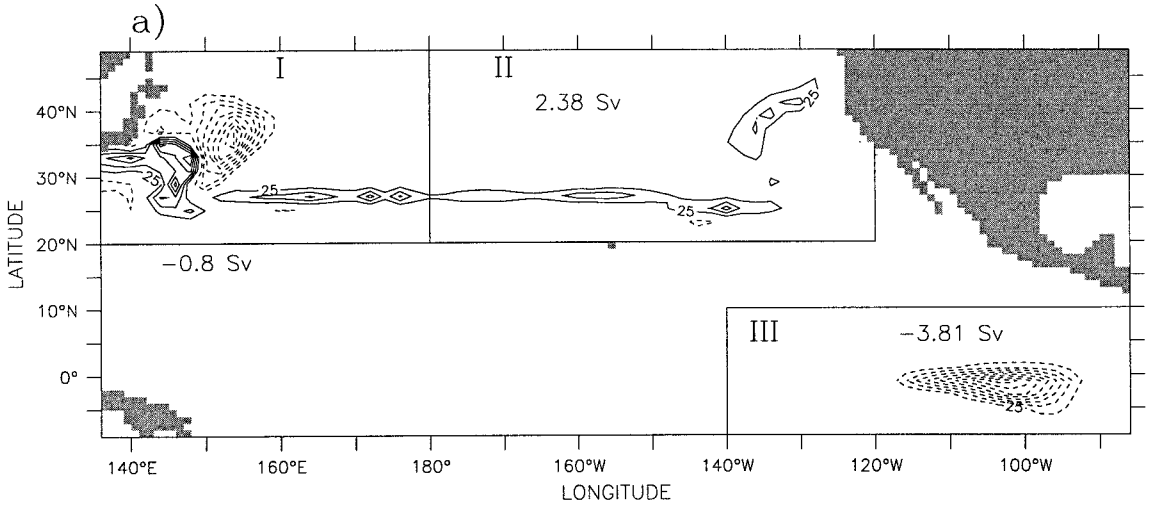

annual flux (m) into layer 7: Total = −2.51 Sv

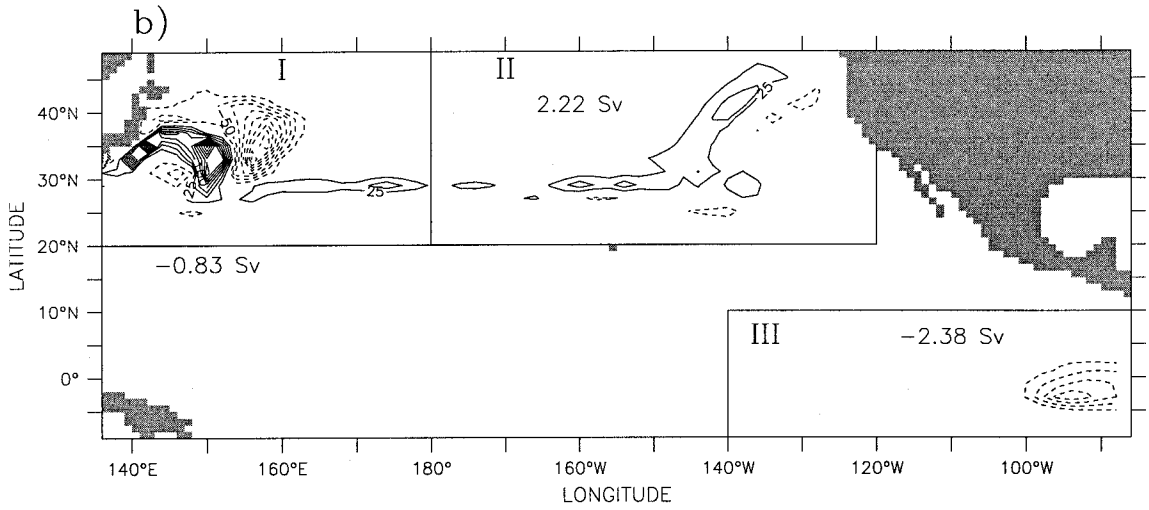

annual flux (m) into layer 8: Total = −1.43 Sv

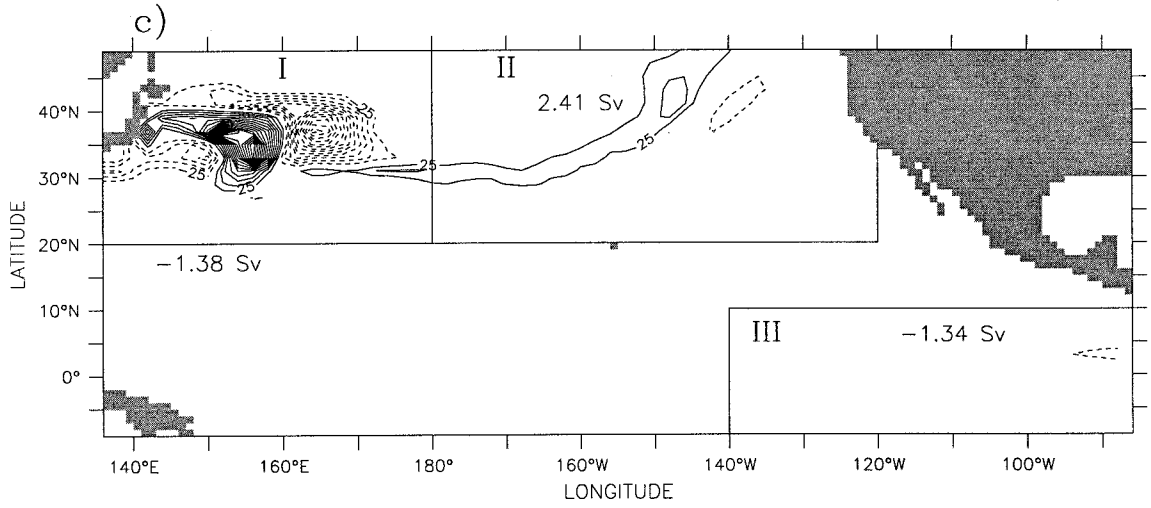

annual flux (m) into layer 9: Total = −0.42 Sv

rameterized as a volume flux between layers. Assuming incompressibility, the volume budget for the isopycnal layer is

$$\left(\frac{\partial \Delta V}{\partial t} + \Delta\Psi\right) = G(\rho) + D(\rho) + D(\rho + \Delta\rho). \quad (5)$$

Thus, the water mass formation for the isopycnal layer consists of layer volume changes and export out of the domain:

$$M\Delta\rho = \frac{\partial \Delta V}{\partial t} + \Delta\Psi, \quad (6)$$

where M is the water mass formation per unit of density. Except for the flux G from the mixed layer in (5), (5) and (6) are the same as Nurser et al.'s (1999) Eqs. (2) and (3). From (4), (5), and (6) we get

$$M(\rho)\Delta\rho = G(\rho) + D(\rho) - D(\rho + \Delta\rho). \quad (7)$$

Thus, water mass formation is related to density flux convergences in the mixed layer and diffusive diapycnal fluxes between isopycnal layers.

4. Transformation rates

Transformation rates [Eq. (3)] are due to both air–sea density fluxes and entrainment density fluxes. Below we calculate these in the model explicitly. First we will discuss transformation and formation rates integrated over the entire model basin. Then, in section 5, we will discuss the details of formation in individual model layers and, in section 6, we will interpret our results in terms of mode water formation.

a. Air–sea density fluxes

Except in the Mediterranean (Tziperman and Speer 1994), studies typically find negative transformation rates at low densities and positive transformation rates at high densities (i.e., net annual cooling where heavier isopycnals outcrop at high latitudes and warming where light isopycnals outcrop in the Tropics). Thus surface density fluxes cause light waters to get lighter and heavy waters to get heavier, increasing the density contrast across the basin.

In isopycnal models, diapycnal volume fluxes (G and D) are calculated at the layer interfaces explicitly. Thus, these models are ideally suited to studies of water mass formation. The total annual mean density flux from net heat flux, freshwater flux, and relaxation flux (1) for year 51 (Fig. 3d) is positive in the Kuroshio Extension region implying that the surface density flux (primarily cooling: Fig. 3a) is acting to increase the density of the sea surface. In a band from 10°S to 10°N, the surface density flux (primarily warming) is acting to reduce sea surface density.

The density flux due to $E - P$ (Fig. 3b) is much weaker than that due to the heat flux (Fig. 3a). However, especially in the Tropics, the $E - P$ density flux is not negligible. Of particular note is the negative density flux in a band along 8°N due to the excess of precipitation over evaporation in the intertropical convergence zone (ITCZ).

The density flux due to the surface density relaxation (Fig. 3c) in the model is of comparable magnitude to the density flux due to heat. Because of errors in the Kuroshio, the relaxation acts to cool the waters of the model Kuroshio Extension. In addition, there is a bullet at about 20°N, 130°W and a band along the eastern equator where the relaxation density flux is acting to lighten the surface waters in opposition to the density flux due to entrainment (Fig. 4). The strong relaxation density flux in the Tropics is due to the limited density resolution at lighter densities and is further discussed below.

The transformation rate can be calculated by using the finite difference form of (3) and summing the density flux over sea surface density bands (Speer and Tziperman 1992):

$$\begin{aligned} F(\rho) &= \frac{1}{\Delta\rho}\sum_{n=1}^{N}\Delta t\sum_{i,j}A_{i,j}[f + w_{\text{entr}}(\rho_k - \rho_{\text{ML}})] \\ &\quad \times \Pi(\rho - \rho') \\ &= F_{\text{heat}} + F_{E-P} + F_{\text{relax}} + F_{\text{entr}}, \end{aligned} \quad (8)$$

where i, j are the model grid indices; A_{ij} is the area of each grid box; N is the total number of time steps (of length Δt) per year; and II is a boxcar function selecting only values in the density range between ρ and ρ'. In this section, we will discuss the part of the transformation rate that is due to surface density fluxes (F_{heat}, F_{E-P}, and F_{relax}). The part of the transformation rate that is due to entrainment from below will be discussed in section 4b.

The annual mean transformation rate due to air–sea density fluxes (Fig. 5) consists of contributions from the heat and $E - P$ flux climatologies (*ASMD*) used to force the model (F_{heat}, F_{E-P}; Fig. 5a) and the relaxation to surface densities (F_{relax}; Fig. 5b). Following Speer and Tziperman (1992), positive values imply a transformation to greater densities. Speer et al. (1995, their Fig. 3b) calculated transformation rates from revised COADS data for the Pacific from 30°S to 70°N. Our calculation for the region from 20°S to 60°N (from a climatology also based on COADS) generally agrees

←

FIG. 10. Total annual flux into model isopycnal layers in meters per year (contour interval: 25 m yr^{-1}). Total flux integrated over regions I, II, and III are shown in Sv for (a) layer 7, (b) layer 8, and (c) layer 9.

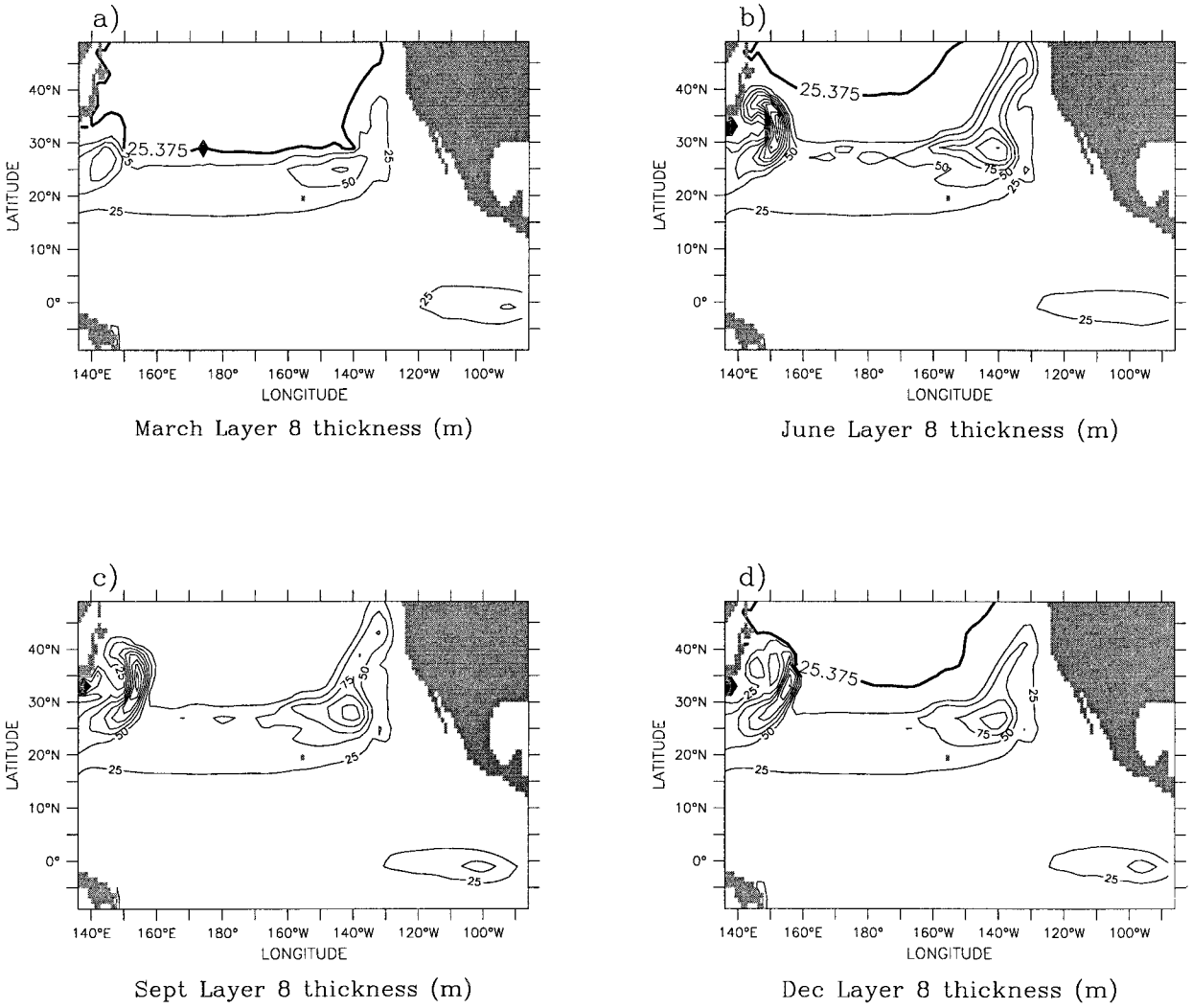

FIG. 11. Layer 8 thickness (contour interval, 25 m). The layer 8 outcrop into the mixed layer is shown as a bold line for (a) Mar, (b) Jun, (c) Sep, and (d) Dec.

with the Speer et al. (1995) calculation within their error bars. However, they do not discuss the relative contributions of heat fluxes and freshwater fluxes to the transformation rates in the North Pacific. In addition, in section 4b, we discuss the effects of entrainment on the transformation rate.

TABLE 2. Formation region, density, and contribution of entrainment density flux convergence to formation rate for the three mode waters.

Mode water	Region	Density (σ_θ) (kg m^{-3})	Percentage of formation rate due to entrainment density flux convergences (%)
STMW	30°–40°N, 150°–160°E	25.75	30
CMW	35°–45°N, 170°E–180°	26.0	8
ESMW	25°–35°N, 150°–140°W	25.5	56

The heat fluxes obviously play the primary role in the transformation rate (Fig. 5a), leading to light ($\sigma_\theta <$ 24.25 kg m^{-3}) surface waters becoming lighter (due to tropical warming) and dense surface waters becoming denser (due to cooling at higher latitudes). However, as seen in Fig. 3, F_{E-P} is not negligible, especially in the lighter density bands. Due to the excess of precipitation over evaporation in the ITCZ (Fig. 3b), F_{E-P} tends to reinforce the effects of tropical warming for density bands lighter than σ_θ = 22.5 kg m^{-3} causing surface waters to become less dense. In the subtropics, evaporation is greater than precipitation. Thus F_{E-P} is positive in the density band $22.5 < \sigma_\theta < 25.5$ kg m^{-3}. In the subpolar gyre ($\sigma_\theta > 25.5$ kg m^{-3}), precipitation exceeds evaporation causing a negative F_{E-P} counteracting the densifying effects of F_{heat}.

Here F_{relax} is positive at low densities and negative at high densities (Fig. 5b), tending to offset the effects of

the climatological forcing. Most of the relaxation density flux is due to two issues mentioned previously. At higher densities, the relaxation can be attributed primarily to the overshoot of the western boundary current. At low to intermediate densities, the relaxation can be attributed to limited density resolution. Because we are primarily interested in the density range of the mode waters of the North Pacific, the vertical resolution at lighter densities is fairly sparse (Table 1). (Any waters lighter than $\sigma_\theta = 22.5$ kg m^{-3} only exist in the mixed layer or the buffer layer.) The limited density resolution causes entrainment density fluxes (Fig. 4) in the Tropics (discussed below) to affect surface densities too strongly, necessitating a negative density flux to offset the entrainment. At the lightest densities ($\sigma_\theta \sim 21$ kg m^{-3}) in the equatorial warm pool of the western tropical Pacific, the mixed layer has very little interaction with the isopycnal layers beneath because the lightest isopycnal layer is 22.5 kg m^{-3}. Thus, the mixed layer continually gets lighter due to surface heat fluxes and the lack of adequate mixing. The positive relaxation density flux at $\sigma_\theta \sim 21$ kg m^{-3} keeps the surface densities in the equatorial warm pool at realistic levels.

b. Entrainment density fluxes

As discussed in sections 2 and 3, mixed layer density is not only affected by the surface density fluxes (Fig. 3), but also by entrainment of isopycnal layer waters from below due to convection and the turbulent kinetic energy supplied by wind mixing and turbulent buoyancy fluxes. We diagnose the density flux from isopycnal layers into the mixed layer. Because the mixed layer is always less dense than the layers below (any static instabilities are erased by convection in one time step), entrainment from an isopycnal layer to the mixed layer due to wind mixing and/or turbulent buoyancy fluxes will lead to densification of the mixed layer. On the other hand, convection occurs when the mixed layer is denser than one or more layers beneath it. Thus convective entrainment leads to lightening of the mixed layer (note that no penetrative convection is included in the model).

While wind mixing occurs over large time and space scales, convective entrainment occurs only during the cooling season and in limited geographical regions. The resulting density fluxes from wind mixing are greater than density fluxes due to convective entrainment. Thus, the change in mixed layer density due to entrainment from below (Fig. 4) is positive almost everywhere.

Due to equatorial upwelling that brings isopycnals closer to the surface, the density fluxes due to mixing are very strong in the equatorial upwelling region, reaching a maximum of 12×10^6 kg m^{-2} s^{-1} between 110° and 120°W. Another weaker maximum can be seen at about 15°N, 125°W under the upwelling-favorable wind stress associated with the ITCZ. As mentioned previously, the density flux due to relaxation (Fig. 3c) partially offsets the entrainment density flux in these two regions.

Transformation due to entrainment (F_{entr}) is positive for all density bands (Fig. 6) with a magnitude comparable to F_{heat}. The peak in transformation rate due to entrainment at $22.5 < \sigma_\theta < 23.5$ kg m^{-3} is due to the strong band of equatorial upwelling seen in Fig. 4. Local effects of entrainment density flux convergences on water mass formation are discussed in section 5.

Walin (1982) showed that mixing is essential in density ranges where air–sea fluxes result in $F(\rho) < 0$ (transformation to lighter densities). In our model, the total transformation rate excluding entrainment ($F_{\text{heat}} + F_{E-P} + F_{\text{relax}}$) is negative for surface densities less than 24.5 kg m^{-3} (Fig. 6). By Walin's reasoning, in this density range, mixing (F_{entr}) has to be large enough to overcome the negative transformation rate. For surface densities greater than 24.5 kg m^{-3}, water is cooled and $F(\rho) > 0$. In this density range, the effects of entrainment on surface density are less important.

5. Formation rates

As seen in (7), water mass formation rates, $M(\rho)$, are due to both density flux convergences in the mixed layer and diapycnal diffusion between isopycnal layers.

a. Density flux convergence

Using the isopycnal model, the part of the formation rate due to density flux convergences can be calculated in two ways: 1) $F(\rho) - F(\rho + \Delta\rho)$, calculated from the model forcing fields and entrainment fluxes, and 2) $G(\rho)$, calculated by the model as the flux out of the buffer layer to the isopycnal layers below. Figure 7 shows $F(\rho) - F(\rho + \Delta\rho)$ (solid line), the flux from the buffer layer to isopycnal layers partitioned by buffer layer density (dashed line), and the flux into isopycnal layers partitioned by the isopycnal layer density (dotted line). The formation rate and diapycnal fluxes represented in Fig. 7 are calculated by averaging over the entire model basin excluding a 10° zone next to the boundaries. The reason we exclude this zone is that the sponge layers at the open boundaries cause diapycnal fluxes near the boundaries that are not related to surface density fluxes.

The flux out of the buffer layer is equal to the flux into the isopycnal layers in total. However, because the flux into the isopycnal layers can only occur at the discrete layer densities, the flux out of the buffer layer (occurring at the continuously varying density of the buffer layer) occurs at different densities than the flux into the isopycnal layers. The formation rate calculated from the transformation rate is very close to the flux from the buffer layer to the subsurface layers. Two peaks in formation are evident at $\sigma_\theta = 22.75$ kg m^{-3} and $\sigma_\theta = 26$–26.25 kg m^{-3} (Fig. 7). The first peak, at $\sigma_\theta = 22.75$ kg m^{-3}, occurs in the Tropics and is not well

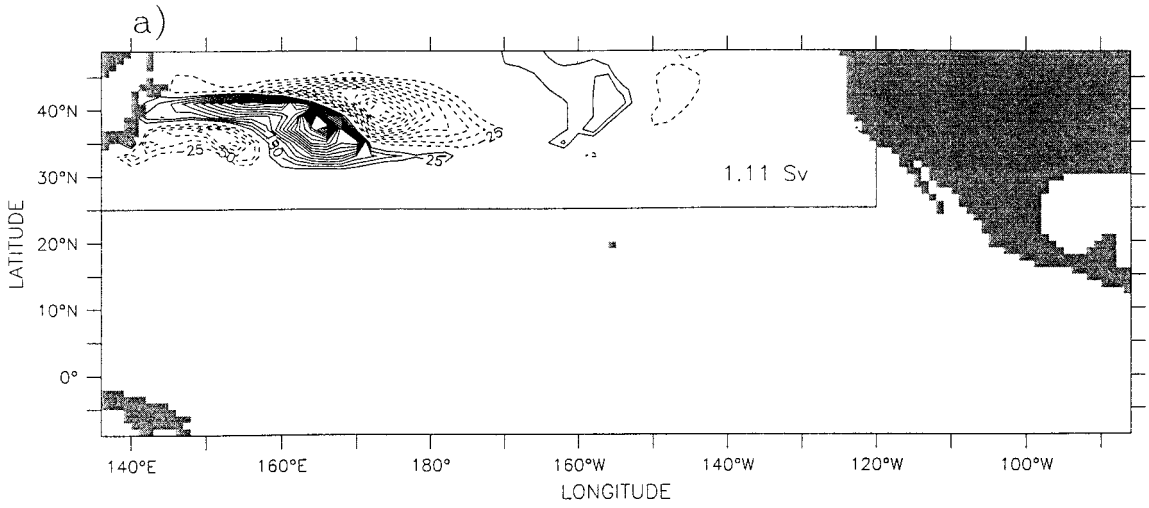

annual flux (m) into layer 10 (Total = −0.08 Sv)

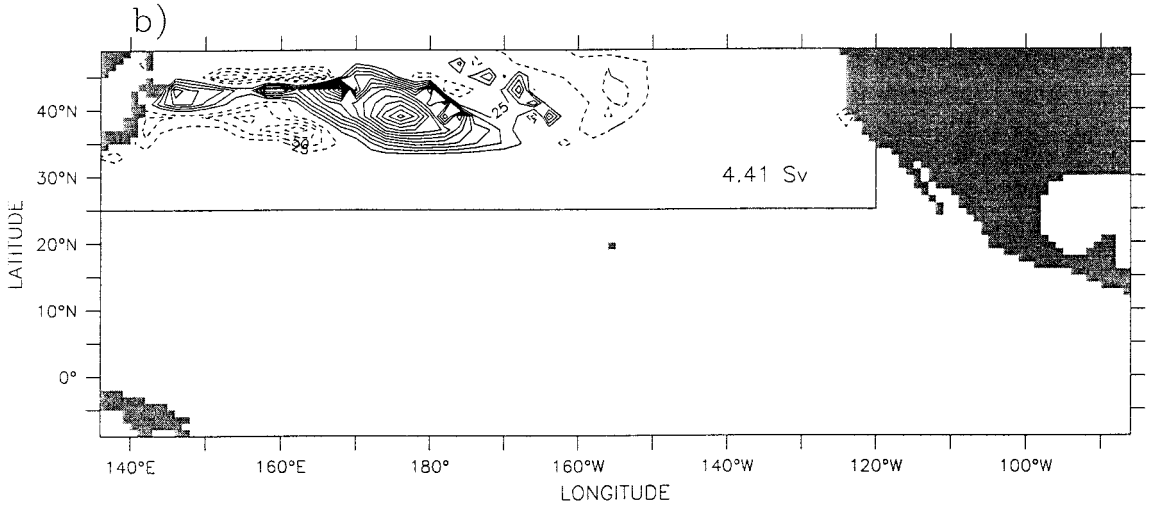

annual flux (m) into layer 11 (Total = 1.51 Sv)

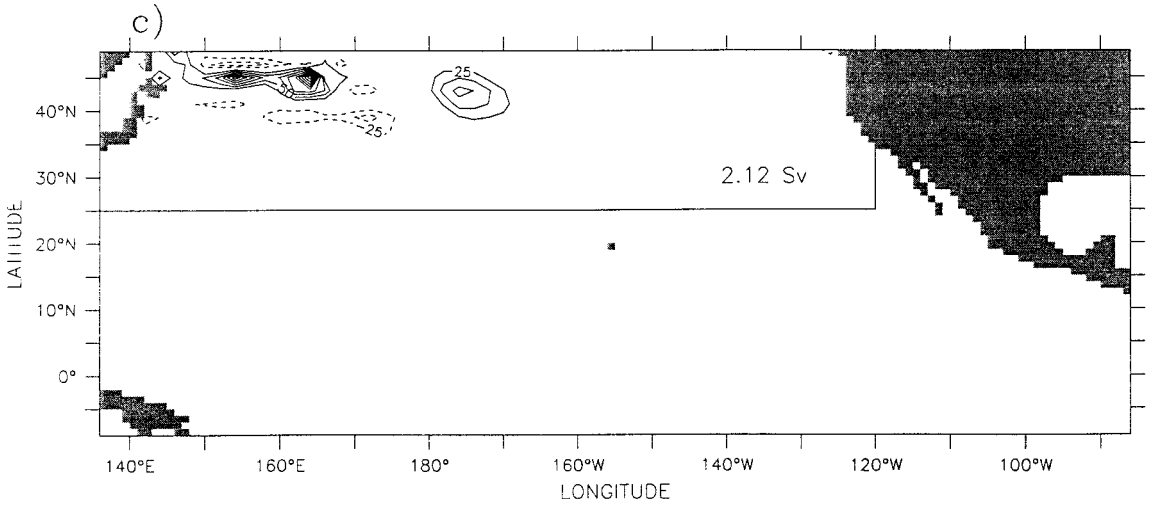

annual flux (m) into layer 12 (Total = 0.54 Sv)

resolved by the sparsely spaced lighter layers of the model as demonstrated by the lack of a peak at this density in the flux into the model isopycnal layers (dotted line). All of the fluxes from the buffer layer occurring between $20.0 < \sigma_\theta < 23.875$ kg m^{-3} can only go into the first two isopycnal layers (layers 3 and 4; Table 1) causing the formation peak at $\sigma_\theta = 22.75$ kg m^{-3} to be smoothed over. The other peak near $\sigma_\theta = 26$ kg m^{-3} is near the density of the CMW. The majority of this formation enters isopycnal layers 9 and 10 with densities of $\sigma_\theta = 25.625$ and 25.875 kg m^{-3}, respectively.

Averages (over smaller regions) of formation due to entrainment density fluxes and formation due to air–sea density fluxes were calculated to gain insight into which of these density fluxes is important to mode water formation. The averages were calculated over 10° square regions surrounding the maximum formation rates in the mode water layers (see Figs. 10 and 12 and section 6). STMW and ESMW formation are due to contributions from both the air–sea density flux and entrainment density flux convergences. On the other hand, entrainment density flux convergences play only a very small role in CMW formation. Table 2 displays a summary of the results of this analysis.

b. Diapycnal diffusion

When averaged over the entire model basin (excluding the 10° boundary zone), the flux into each isopycnal layer due to diapycnal diffusion has a large effect on the total formation (Fig. 8) tending to smooth out the effects of the mixed layer density fluxes. Of particular interest is that after including the effects of diffusion, layer 10 ($\sigma_\theta = 25.875$ kg m^{-3}) formation is almost zero while layer 11 formation is positive. Thus, after the effects of diffusion are included, CMW forms in layer 11 with a density of $\sigma_\theta = 26.125$ kg m^{-3} [closer to the observationally determined CMW density of $\sigma_\theta = 26.25$ kg m^{-3}, Nakamura (1996)].

6. Mode waters

Now we turn our attention to a description of mode water formation in the model. We will relate the water mass formation rates discussed in section 5 to the formation of mode water. Mode water can be identified and traced using its signature low potential vorticity (McCartney 1982). The model calculates PV in each layer as

$$\mathrm{PV}_k = \frac{\Delta\rho}{\rho_k}\left(\frac{f + \zeta}{h}\right), \tag{9}$$

where k is the layer index, $\Delta\rho$ is the difference ($\rho_{k+1/2} - \rho_{k-1/2}$) between the interface densities, f is the planetary vorticity, ζ is the relative vorticity, and h is the layer thickness. The zonal distribution of annual mean PV along 29°N calculated by the model (Fig. 9) looks much like that calculated from Levitus climatology (Ladd and Thompson 2000, see their Fig. 4) although PV calculated from the model tends to be smaller due to the limited vertical resolution. A large minimum in PV ($<2.0 \times 10^{-10}$ m^{-1} s^{-1}) in the central Pacific appears lighter and shallower in the west, existing in layer 8 ($\sigma_\theta = 25.375$ kg m^{-3}) at 150°E, and deeper and denser in the east reaching layer 11 ($\sigma_\theta = 26.125$ kg m^{-3}) as far east as 150°W. This PV minimum is a feature of the STMW in the lighter layers in the western Pacific and the CMW in the deeper layers in the central and eastern Pacific. Nakamura (1996) identifies STMW on the $\sigma_\theta = 25.5$ kg m^{-3} isopycnal and CMW on the $\sigma_\theta = 26.25$ kg m^{-3} isopycnal, consistent with our model results given our limited vertical resolution.

A second weaker and shallower PV minimum ($<3.0 \times 10^{-10}$ m^{-1} s^{-1}) can be seen in layers 7 and 8 in the eastern Pacific (approximately 140°W) at a depth of slightly more than 100 m. As noted by Ladd and Thompson (2000), this is a feature of the ESMW. Hautala and Roemmich (1998) calculate a density range of 24.0–25.4 kg m^{-3} for the ESMW, consistent with our model results (layer 7 $\sigma_\theta = 25.125$ kg m^{-3}, layer 8 $\sigma_\theta = 25.375$ kg m^{-3}).

By looking at the regional variation of formation in specific layers, we can gain an understanding of how the mode waters in individual layers are formed and the relationships between layers. To understand formation in layers 7, 8, and 9, (25.125 kg m$^{-3} < \sigma_\theta < 25.625$ kg m^{-3}, the traditional density range of STMW) we have divided the basin into three regions (I, II, and III) (Fig. 10).

a. Subtropical Mode Water

Region I, in the western Pacific near Japan, includes the model STMW formation region. This region exhibits net negative formation for all three layers (Fig. 10). However, the very strong local maximum in formation in layers 8 and 9 at approximately 150°E contributes to the STMW PV minimum (thickness maximum) there (Figs. 9 and 11).

We define the STMW region to be the region 15°–50°N, 135°E–180°, enclosing the western thickness maximum (PV minimum) apparent in Fig. 11. Next, we define STMW as any layer 7–9 water in the STMW region that has PV less than 2.0×10^{-10} m^{-1} s^{-1}. This

←

FIG. 12. Total annual flux into model isopycnal layers in meters per year (contour interval: 25 m yr^{-1}). Total flux integrated over region north of 25°N shown in Sv for (a) layer 10, (b) layer 11, and (c) layer 12.

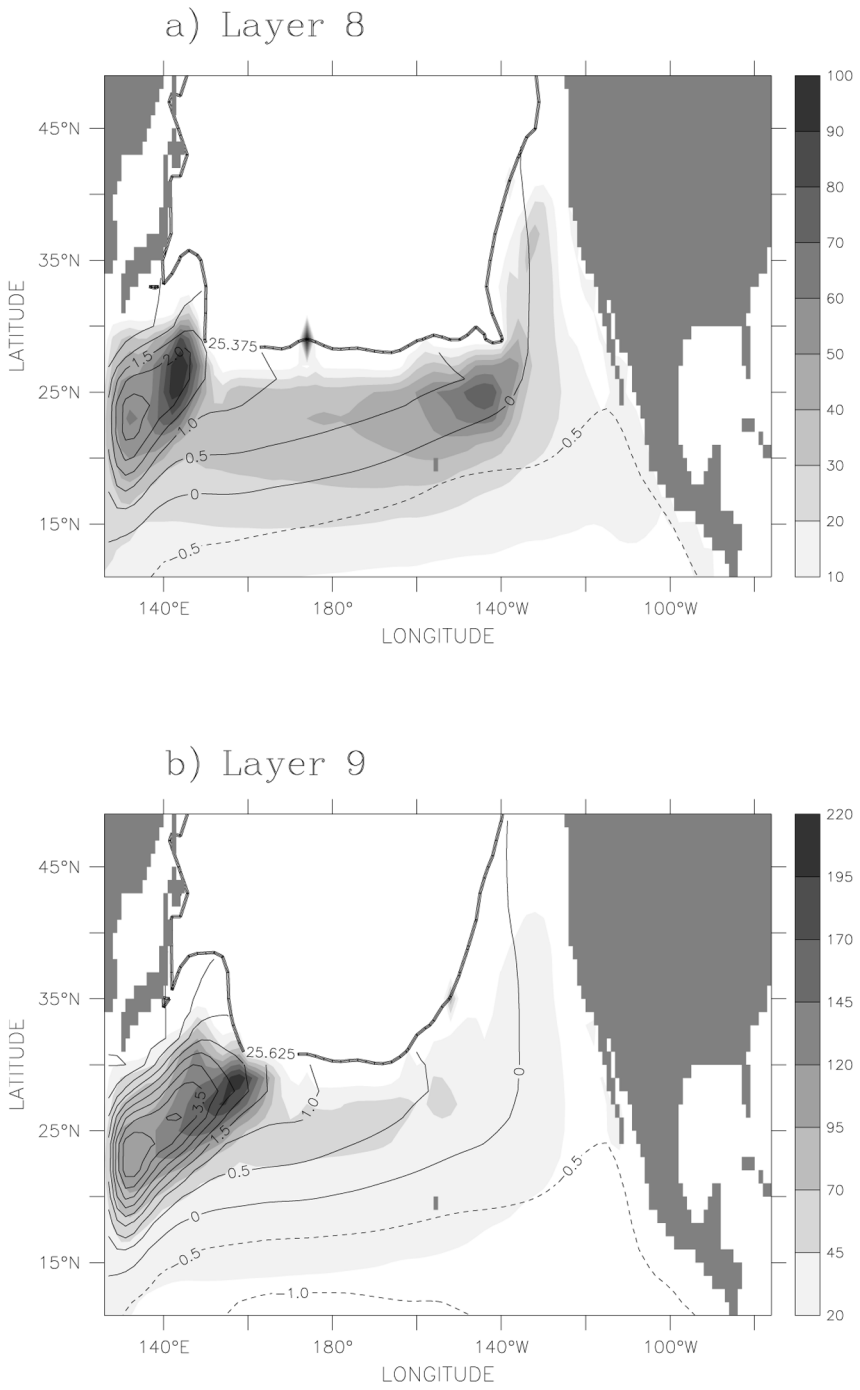

FIG. 13. Layer streamfunction (thin contours) superimposed on Mar layer thickness (gray shading). Bold line denotes Mar outcrop location for (a) layer 8 (σ_θ = 25.375 kg m^{-3}) and (b) layer 9 (σ_θ = 25.625 kg m^{-3}).

PV restriction causes most of the volume used in the calculation to be in layer 9. Only a small region of layer 7 satisfies the PV requirement.

Using this STMW definition, the volume of STMW ranges from a minimum of 3.2 $\times$ 10^{14} m^3 in March when the mixed layer is the deepest to a maximum of 9.7 $\times$ 10^{14} m^3 in June, when the mixed layer has detrained most of its water into the isopycnal layers. Assuming no PV diffusion, the ratio of minimum to maximum volume implies that 33% of the mode water escapes south of the outcrop so that it will not be reentrained the next winter. The annual average formation

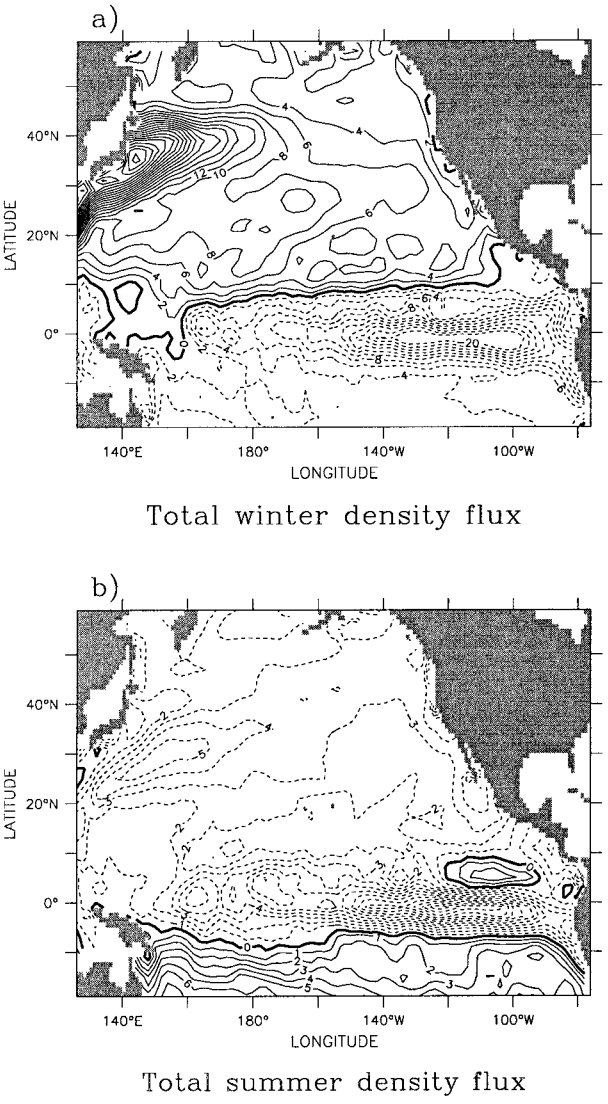

FIG. 14. Seasonal density flux in model year 51 (contour interval: 1.0×10^6 kg s^{-1} m^{-2}) during (a) winter (Oct–Mar) and (b) summer (Apr–Sep).

rate integrated over this region for layers 7–9 is negative. However, the negative formation does not contribute to STMW formation. If we integrate over just the positive formation rates, we get a STMW formation rate of 7.1 Sv. Dividing the minimum STMW volume by the formation rate gives a renewal time of roughly 1.5 years. This is consistent with ages of less than 2 years calculated from apparent oxygen utilization values (Suga et al. 1989). Using the average mode water volume gives a renewal time of 5.5 years. (See Table 3 for a comparison of the formation rates, renewal times, and percent of volume escaping reentrainment for the three mode water masses.)

In contrast, Huang and Qiu (1994) calculate a renewal time of 6.8 yr for water in the North Pacific west of the date line in the STMW density range (σ_θ = 25.2–25.4 kg m^{-3}). Because their calculation includes all water west of the date line in that density class, it averages the mode water pycnostad with the rest of the water in the same density class. Thus, the volume is larger and the ventilation rate is smaller, leading to the longer renewal time. Discrepancies between our renewal time and that calculated by Huang and Qiu can be accounted for by the differences in mode water definition regions used in the calculation, and by the fact that, due to low horizontal resolution, the model underrepresents the recirculation.

TABLE 3. Summary of formation rate, renewal time, and percent escaping reentrainment for the three mode waters.

Mode water	Formation rate (Sv)	Renewal time (yr)	Volume escaping reentrainment (%)
STMW	7.1	1.5–5.5	33
CMW	7.6	10–14	61
ESMW	5.8	0.5–1.5	13

Now we will look at the fate of the water as it moves through the STMW formation region. As warm surface water is carried north by the Kuroshio, it gets denser due to air–sea density fluxes (Fig. 3d). At about 30°N, 145°E, water enters layer 7 resulting in a maximum in layer 7 formation of over 100 m yr^{-1} (Fig. 10a). As the water continues to move northeastward into regions of deeper winter mixed layers (Fig. 1), it gets reentrained into the mixed layer during the next cooling season where it can cool further. This explains the region of negative formation ($>$150 m yr^{-1}) downstream of the positive formation maximum (Fig. 10a). By the next mixed layer detrainment season, it has cooled enough to enter layer 8, resulting in a formation maximum in layer 8 of approximately 200 m yr^{-1} (Fig. 10b) that is downstream of the maximum (and overlaps part of the negative formation region) in layer 7. The same pattern is repeated with water from layer 8 being entrained into the mixed layer, cooling further, and entering layer 9 (maximum formation $>$300 m yr^{-1}: Fig. 10c). Thus, each successively deeper layer exhibits the same pattern (negative formation downstream of positive formation) downstream of the layer above. This pattern continues in layer 10 (Fig. 12) to be discussed below. Similar patterns are found in a model of mode water formation in the North Atlantic (Marsh and New 1996). Thus, preconditioning of the water in the western part of the STMW formation region, with water becoming successively cooler and denser with each season, is of importance in formation of the denser varieties of STMW formed farther to the east. This preconditioning pattern is consistent with Talley's (1988) finding that the PV minimum of the STMW is found at increasing density from west to east.

Now, we describe the seasonal cycle of formation. Because layer 8 can be used to illustrate both the STMW and the ESMW distributions and layer 9 in the STMW

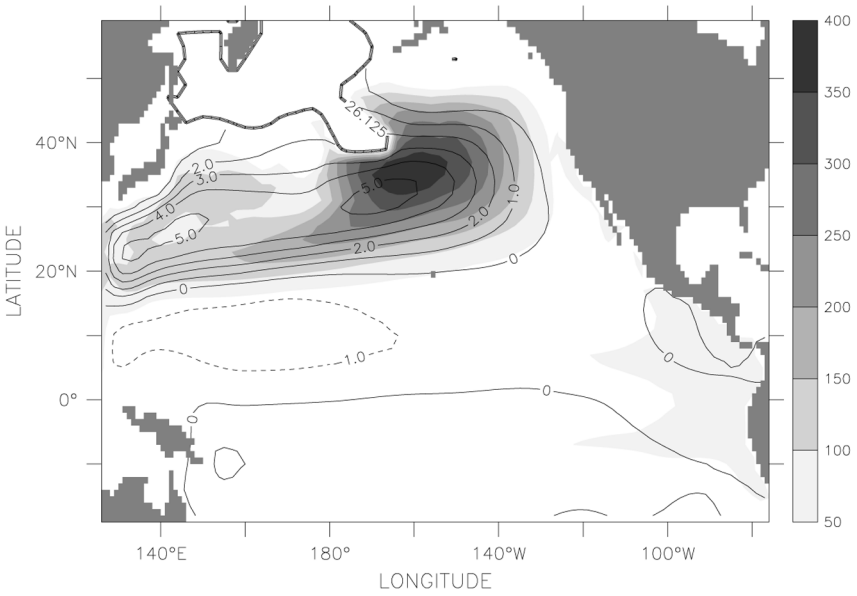

FIG. 15. March layer 11 streamfunction (thin contours) superimposed on layer 11 thickness (gray shading). Bold line denotes σ_θ = 26.125 kg m^{-3} (nominal density of layer 11) outcrop location.

region looks similar to layer 8, layer 8 is used in the following discussion. In March, the mixed layer is the deepest (Fig. 1) and layer 8 is the thinnest (Fig. 11a). The layer 8 outcrop lies along ~30°N in the central Pacific, its southernmost location of the year. The western maximum in March layer 8 thickness (>75 m) is the remains of STMW formed during the mixed layer shoaling of the previous summer. As the ocean surface warms during the summer, the outcrop location moves north. By June, the layer 8 outcrop has moved to ~40°N (Fig. 11b). As the mixed layer warms, it shoals and detrains mixed layer water into the isopycnal layers below. This results in the formation maximum at roughly 35°N, 150°E and the large layer 8 thickness (maxima of ~250 m in the west) in the model during summer and early autumn. The thickness maximum apparent in June recirculates tightly in the western part of layer 8. In September, the mixed layer is lighter than 25.375 kg m^{-3} everywhere and the isopycnal outcrop does not appear in Fig. 11c. By December, the mixed layer has started cooling and entraining layer 8 water, eroding away the thickness of layer 8 until, in March, the remaining thickness maximum is much weaker and consists of only the part of the thickness maximum that has circulated to the south of the winter outcrop location.

The negative net formation in layer 8 region I suggests that most of the thickness maximum formed in layer 8 during the winter is reentrained into the mixed layer and further cooled to form layer 9 water. Thus, the year-round existence of STMW in layer 8 is dependent on the tight circulation that allows part of the thickness maximum to be carried south of the outcrop location before the next year's cooling season.

The layer streamfunction superimposed on March layer thickness (Fig. 13) illustrates the tight circulation pattern of the STMW after formation. The circulation is tighter and more confined to the northwest corner of the gyre in layer 8 (Fig. 13a) than in layer 9 (Fig. 13b). Again we emphasize that the recirculation is underestimated in the model. If properly represented, nonlinear effects and eddies would increase the recirculation and thus increase residence time of the mode water by allowing more mode water to escape reentrainment. In fact, Hazeleger and Drijfhout (2000) find that subduction in the 18° Water formation region in the North Atlantic is enhanced in an eddy-resolving model as compared to the results of a non-eddy-resolving model.

Fine et al. (1994) find evidence of STMW [PV minima, chlorofluorocarbon and tritium maxima] as far south as 10°N in the Mindanao Current. The PV minima and tracer maxima correspond to a density range between 25.4 and 25.6 kg m^{-3}. This density range implies that the STMW that reaches the Mindanao Current is formed in the eastern part (east of 150°E) of the STMW formation region (Bingham 1992) and recirculated on the outer edge of the subtropical gyre before being entrained into the current. Our results support this hypothesis by showing that the denser STMW such as that formed in layer 9 (Fig. 13b) is more likely to reach as far south as 10°N.

b. Eastern Subtropical Mode Water

Region II exhibits positive formation (>25 m yr^{-1}) for layers 7, 8, and 9 (Fig. 10). The band of positive formation occurs along the March layer outcrop where

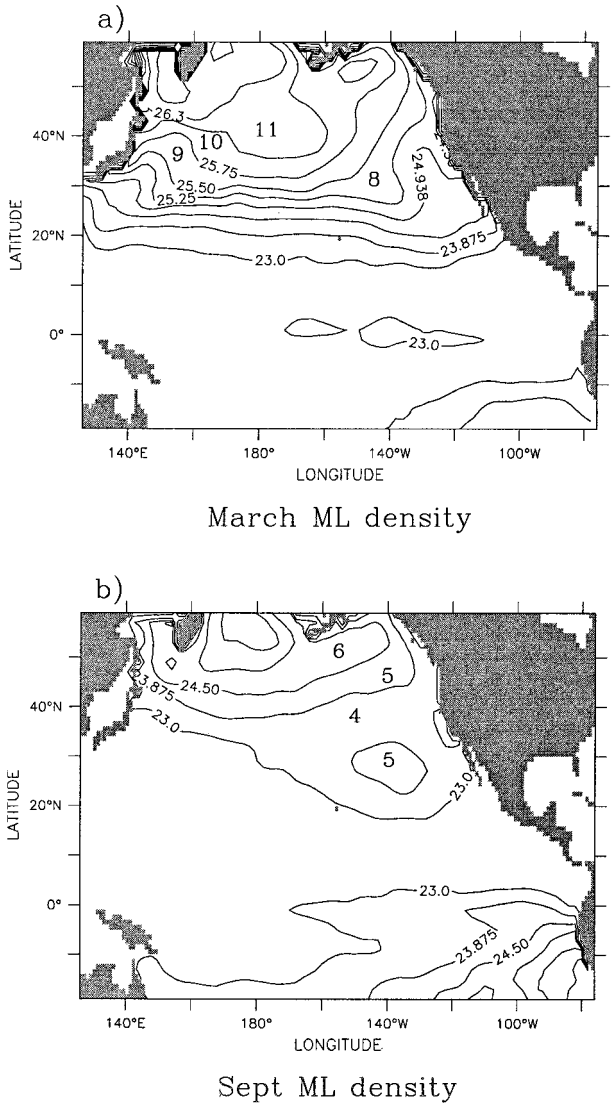

FIG. 16. Mixed layer density. Contours represent the interfaces between isopycnal layers. Thus area between contours denotes the model isopycnal layer outcrop region in (a) Mar (numbers 8–11 indicate layer indices) and (b) Sep (numbers 4–6 indicate layer indices).

water gets detrained from the mixed layer into the isopycnal layer as the mixed layer starts to warm during the early spring. The eastern end of region II is the ESMW formation region.

We define the ESMW region to be the region 15°–50°N, 170°–120°W, enclosing the eastern thickness maximum (PV minimum) in Fig. 11. Next, we define ESMW as any layer 6–8 water in the ESMW region that has PV less than 3.0×10^{-10} m^{-1} s^{-1}. Using this definition, the volume of ESMW ranges from a minimum of 6.8×10^{13} m^3 in March to a maximum of 50.8×10^{13} m^3 in June. That the minimum volume is an order of magnitude less than the maximum volume implies that the PV minimum mode water volume does not move very far from the formation region before the mixed layer deepens again, eroding it away. Formation rate, renewal time, and percentage of ESMW escaping reentrainment are summarized in Table 3.

As layer 8 is the primary ESMW layer, we will concentrate on layer 8 for the remainder of the ESMW discussion. In the formation region, relatively weak summer heating (note the −3 contour in Fig. 14b) leads to a local surface density maximum at the end of the summer (Fig. 16b). This allows the $\sigma_\theta = 25.5$ kg m^{-3} isopycnal to move farther to the southeast in this region during winter cooling, creating a wide layer 8 outcrop in summer (Fig. 16a). The wide surface outcrop is related to the subsurface ''stability gap''—a lateral minimum in the vertical stability—discussed by Roden (1970, 1972) and Yuan and Talley (1996). The influence of weak summer heating on ESMW formation is discussed by Ladd and Thompson (2000). Since the net formation of isopycnal layer water can be represented as the formation rate integrated over the width of the outcrop, the local thickness of the layer is dependent on both the formation rate and the width of the outcrop. The positive formation in region II, coupled with the wide outcrop around 150°W, results in a layer 8 thickness maximum (the ESMW) at approximately 140°W (Fig. 11).

ESMW formed in the eastern part of layer 8 recirculates with a much longer trajectory than the STMW does in the west (Fig. 13). Slow current speeds in the eastern part of the basin contribute to the short renewal time of the ESMW. Because the renewal time for ESMW is less than one year, it is unlikely that any ESMW signal could reach very far from the formation region.

Region III includes the equatorial upwelling region where formation rates are negative (Fig. 10). Successively denser layers upwell (exiting the isopycnal layer) farther to the east. Since layer thicknesses are not changing from year to year, the negative total formation rates in layers 6, 7, and 8 (Figs. 8 and 10) imply a source of waters at these densities through the open boundaries of the model.

c. Central Mode Water

We define the CMW region as 15°–50°N, 140°E–120°W, encompassing the thickness maximum (PV minimum) in Fig. 15. Next, we define CMW to be any layer 10–12 water in this region that has PV less than 1.0×10^{-10} m^{-1} s^{-1}. Layer 11 is the primary CMW layer. The PV restriction used in the definition of CMW is more restrictive than was used for ESMW and STMW since the PV minimum for CMW is much stronger than for the others. Using this definition, the volume of CMW ranges from a minimum of 2.3×10^{15} m^3 in March to a maximum of 3.8×10^{15} m^3 in June. The annually averaged volume is 3.3×10^{15} m^3. These volumes exceed the volumes of the ESMW and the STMW by an order of magnitude even with the more restrictive definition of CMW. For comparison, annual average vol-

umes of 1.4×10^{15} m^3 (CMW) and 5.2×10^{14} m^3 (STMW) are calculated from climatological data (Levitus et al. 1994; Levitus and Boyer 1994). Formation rates and renewal times are summarized in Table 3. The renewal time for CMW is consistent with the 10–15-yr ventilation timescale calculated by Warner et al. (1996) on the $\sigma_\theta = 26.0$ kg m^{-3} surface using *p*CFC apparent ages.

As noted previously, preconditioning in the western part of the STMW formation region contributes to formation of denser STMW farther to the east. Formation in layer 10 ($\sigma_\theta = 25.875$ kg m^{-3}) shows the same pattern as region I formation for layers 7, 8, and 9 (Figs. 12a and 10) with negative formation exhibited downstream of positive formation. This suggests that the preconditioning supplied by the STMW formation may contribute to formation of CMW. However, due to the limited horizontal resolution of the model, the fronts associated with the Kuroshio Extension are not adequately resolved. Nakamura (1996) showed that STMW formation occurs south of the main path of the Kuroshio Extension while CMW is formed north of it. This deficiency of the model needs further discussion.

The observed mixed layer depth distribution (Fig. 1b) illustrates the separation of the two mode water formation regions. The region of mixed layer depths greater than 150 m at about 32°N, 150°E (smaller shaded area in Fig. 1b) corresponds to the STMW formation region. Just north of this region at about 35°N, mixed layer depths shallower than 150 m (unshaded) correspond to the main path of the Kuroshio Extension as it separates from the boundary. At 40°N, the zonal band of mixed layers deeper than 200 m (larger shaded area) corresponds to the CMW formation region. On the other hand, mixed layer depths computed by the model (Fig. 1a) show a much broader pattern of deep mixed layers encompassing both mode water formation regions. Thus, the implication that STMW formation preconditions the water column allowing CMW to form is probably an artifact of the limited horizontal resolution of the model. However, preconditioning from mode waters formed farther to the west is important in the formation of denser varieties of mode water formed farther to the east for both STMW and CMW. This aspect of the model is likely to be realistic and represents an important process.

Using a high-resolution model, de Miranda et al. (1999) find an analogous situation in the South Atlantic. Their model generates progressively denser mode waters toward the east. In addition, they find that the eddy kinetic energy in the Brazil Current–Malvinas Current Confluence region is too intense to allow a direct connection between deep convection in the western boundary current and those in the open South Atlantic where mode water is formed. However, eddies in the confluence region precondition the water column for convection.

Keeping in mind these problems, we examine the formation of CMW. Formation in layer 10 (Fig. 12a) is positive when integrated over the region north of 25°N. However, due to diffusion in the rest of the basin, the formation in layer 10 is negative when integrated over the entire model basin. On the other hand, layer 11 formation (Fig. 12b) is strongly positive (4.4 Sv) when integrated over the region north of 25°N. Although diffusion in the rest of the basin erodes away this positive formation, the net formation over the whole model basin is still positive (1.5 Sv) (Figs. 12b and 8). The region of maximum positive formation in layer 11 is the CMW formation region (in addition, layer 12 has a small localized region of CMW formation). The CMW formation region can also be seen in the March outcrop location for layer 11 (Fig. 16a), which surrounds the region of positive formation.

The thickness of layer 11 in March (Fig. 15) shows where the mixed layer has entrained some layer 11 water in the northwest corner of the basin, especially around 40°–45°N, 180°–170°W at the eastern end of the formation region (Fig. 12). This region also coincides with the mixed layer depth front at the eastern edge of the mixed layer depth maximum (Fig. 1). Inui et al. (1999) note that low PV water exits the mixed layer and penetrates into a subsurface layer at the point where an outcrop line intersects the mixed layer depth front.

The circulation pathways in layer 11, as illustrated by the streamfunction contours (Fig. 15), show how the CMW circulates after formation. The layer thickness contours wrap around the gyre with the maximum diffusing away as it gets farther from the formation region. The southern arm of the circulation flows to the west, hitting the western boundary between approximately 15° and 20°N. Most of the CMW signal turns north in the western boundary current affecting the subtropical gyre. However, a very small portion of the CMW thickness maximum turns south. In fact, when they reach the western boundary, the streamfunction contours in the range $-1.0 < \psi < 0.0$ turn south to join the equatorial circulation. If diffusion does not completely wipe out the CMW signal, mode water formed in the eastern part of the formation region and circulating along these streamfunctions could potentially reach the equator. Thus, CMW may play a role in subtropical–tropical exchange. However, the lack of negative formation in layer 11 along the equator (Fig. 12) [such as that seen in region III of layers 7 and 8 (Fig. 10)] suggests that the CMW may be too deep to influence the equatorial upwelling and air–sea interaction. In fact, densities of the equatorial pycnocline calculated from the Levitus climatology are in the range $23.5 < \sigma_\theta < 26$ kg m^{-3}, shallower than the CMW density of $\sigma_\theta \sim 26.2$ kg m^{-3}.

7. Summary and conclusions

An isopycnal model was used to examine water mass transformation and formation in the North Pacific. Traditionally, transformation rates have been calculated

from air–sea flux data to gain information on how air–sea density fluxes affect the mass of water in certain density classes. In addition, by considering a steady state in a closed region, average diapycnal diffusion can be estimated (e.g., Speer 1997). We have taken an alternate approach by looking at limited regions in a model of the North Pacific that include fluxes into/out of the region and assuming we can accurately model the diffusion. Then the combination of formation due to air–sea density fluxes and formation due to entrainment and diffusion can give information about how water in certain density classes is formed and destroyed. This regional formation information can be applied to investigate the formation of mode waters in the North Pacific.

Transformation rate, the rate at which surface water is transformed from one density to another, is a function of air–sea density fluxes and entrainment from below. The transformation rate due to air–sea density fluxes is dominated by the effects of the heat flux with surface densities less (greater) than 24.25 kg m^{-3} getting lighter (denser). However, the effects of $E - P$ are not negligible, with $E - P$ acting to reinforce the effects of tropical warming for surface densities less than 22.5 kg m^{-3}. For surface densities between 22.5 and 25.5 kg m^{-3}, the excess of evaporation over precipitation in the subtropical gyre causes transformation rates owing to $E - P$ to be positive. In the subpolar gyre ($\sigma_\theta > 25.5$ kg m^{-3}), the opposite case applies.

Transformation due to entrainment from below is positive for all density classes and comparable in magnitude to the transformation due to heat fluxes. A peak in transformation due to entrainment in the density range $22.5 < \sigma_\theta < 23.5$ kg m^{-3} is due to a strong band of equatorial upwelling causing the densification of surface waters.

Formation rates can be calculated from convergences in transformation and diapycnal diffusion. When annual formation rates are averaged over the entire North Pacific, a large peak in water mass formation is found at a density of approximately $\sigma_\theta = 26$ kg m^{-3}. This peak in formation rate corresponds to the formation of North Pacific CMW in the model. No corresponding peaks in formation rate are found for the STMW or the ESMW when averaged over the entire model basin. However, when calculated locally, enhanced formation rates are found at the densities of these mode water masses.

In a $10° \times 10°$ region corresponding to STMW, a maximum in formation is found at $\sigma_\theta = 25.75$ kg m^{-3} of which 30% is due to convergences in density fluxes due to entrainment while 70% is due to air–sea density flux convergences. In a region corresponding to ESMW, a formation maximum is found at $\sigma_\theta = 25.5$ kg m^{-3} (56% due to entrainment). In contrast, the formation of CMW (maximum formation at $\sigma_\theta = 26$ kg m^{-3}) is due almost entirely to air–sea density flux convergences.

As expected, STMW formation is dependent on the strong cooling and resultant deep mixed layers southeast of the Kuroshio Extension. However, negative formation rates in the STMW formation region imply that most of the thickness maximum formed there each winter is subsequently reentrained into the mixed layer where it is further cooled, preconditioning it to become a denser variety of STMW. That a thickness maximum remains in the region in the next winter is due to the tight circulation that carries the mode water south of the March isopycnal outcrop before the mixed layer cools enough to reentrain it. The renewal time of the STMW is in the range 1.5–5.5 years.

ESMW formation occurs as a band of positive weak formation along the March outcrop. This weak formation, combined with a wide layer outcrop, results in the ESMW layer thickness maxima (PV minima). As discussed by Ladd and Thompson (2000), the wide layer outcrop is at least partially due to weak summer heating in the southeastern part of the formation region. The annually averaged ESMW formation rate is about 5.8 Sv. The renewal time of the ESMW is in the range 136–619 days. The minimum annual volume of ESMW is only about 13% of the maximum volume implying that 87% of the ESMW volume gets eroded away during the winter mixed layer deepening. In comparison, the minimum STMW volume is 33% of the maximum and the minimum CMW volume is 61% of the maximum. Due to the tighter recirculations and faster currents in the central and western Pacific as opposed to the eastern Pacific, a larger percentage of the CMW and the STMW escapes reentrainment.

ESMW formed in previous years and then reentrained into the mixed layer to form new ESMW may effect the properties of the currently forming mode waters. Namias and Born (1970, 1974) noted a tendency for midlatitude SST anomalies to recur in succeeding winters without persisting through the intervening summer. They speculated that temperature anomalies in the deep winter mixed layer could remain intact in the seasonal thermocline during the summer, insulated from surface processes by the shallow summer stratification. These anomalies could then affect the temperature of the succeeding winter's deep mixed layer. Results from a one-dimensional mixed layer model support the Namias and Born hypothesis (Alexander and Deser 1995). However, using a three-dimensional model of the North Pacific, Miller et al. (1994) find that this reemergence mechanism is weak over most of the central Pacific (in the region of the California Current and the Kuroshio Extension) but does occur in the vicinity of the ESMW formation region. The large volume of mode water that is reentrained into the mixed layer every year could explain why the Namias and Born mechanism occurs in this region.

Formation of CMW is dependent on preconditioning supplied by the formation of deep mixed layers west of the CMW formation region. The annual average volume of CMW is 4 times greater than the average volume of STMW and 10 times greater than the volume of ESMW. This large volume results in a renewal time of the CMW

of 10–15 years, consistent with ventilation times calculated from *p*CFC apparent ages (Warner et al. 1996).

The formation of mode water allows SST anomalies to subduct, isolating them from further contact with the atmosphere. If the anomalies circulate with the mode water and are reentrained back into the mixed layer at some future time (and place), then they may once again influence the atmosphere. Thus, mode water formation plays a role in the ''memory'' of the ocean–atmosphere system. Because of the short residence times of the STMW and ESMW, they are most likely to affect air–sea interaction locally. On the other hand, CMW, with its long residence time, may play a role in air–sea interaction remote from its formation region.

Recent studies have suggested that water parcels subducted in the subtropical North Pacific may provide a link between the midlatitude and the tropical ocean. This link may influence subtropical and tropical variability on decadal timescales (Gu and Philander 1997; Zhang et al. 1998). Subducted thermal anomalies can propagate equatorward in the thermocline (Gu and Philander 1997; Schneider et al. 1999), eventually upwelling and affecting sea surface temperatures in the Tropics and perhaps the frequency or magnitude of El Niño events. The atmosphere could then respond to the anomalous SST and, through teleconnections (Bjerknes 1966; Alexander 1992; Philander 1990), affect the surface ocean in the subtropics; thus influencing decadal variability. Schneider et al. (1999), using a dataset of BT, XBT, and CTD stations compiled by White (1995), succeed in tracking anomalies in the depth of the 12°–18°C isothermal layer (a range that includes both CMW and STMW temperatures) from the central North Pacific to approximately 18°N. They calculate a travel time of approximately eight years from the central North Pacific to the subtropical western Pacific. However, south of 18°N, Schneider et al. find that the thermal anomalies are primarily forced by the local wind stress curl and do not originate in the North Pacific. Using an ocean general circulation model, Nonaka et al. (2000) find that the signal from an SST anomaly initiated in the central North Pacific reaches the equator, but with a magnitude reduced to less than 10% of the midlatitude anomaly.

Because STMW is formed in, and primarily confined to, the recirculation region of the western subtropical gyre, only the densest varieties of STMW (formed farthest to the east) are likely to participate in the subtropical–tropical exchange. General circulation models have been used to deduce the pathways taken by subducted water parcels (Gu and Philander 1997). Results suggest that the water masses formed farther to the east, such as the ESMW and the eastern part of the CMW, are the most likely to have an influence on the Tropics. Our results suggest that, due to the slow circulation in the eastern part of the subtropical gyre, most of the ESMW volume does not escape reentrainment into the mixed layer in the succeeding winter. This makes it less likely that variations in water properties introduced with the ESMW can move far from the formation region. In addition, due to the Namias and Born (1970, 1974) mechanism, the ESMW properties may be some kind of average over several years of ESMW formation. Thus, CMW is probably the most likely of the North Pacific mode waters to influence the Tropics. However, CMW, with $\sigma_\theta \sim 26.2$ kg m^{-3}, is deeper than the equatorial pycnocline, suggesting that it may not have any influence on tropical air–sea interaction.

Due to the role of mode water formation in air–sea interaction both locally in the midlatitudes and remotely in the Tropics, an understanding of the circulation and variability of these mode waters may be important to our understanding of decadal variability. The analysis presented here of the modeled climatological formation of mode waters in the North Pacific gives us a baseline for further studies of the effects of variability on mode water formation.

Acknowledgments. We are grateful to Susan Hautala, Sabine Mecking, and David Darr for many helpful discussions. Suggestions by two anonymous reviewers greatly improved this manuscript. This work was supported by the National Aeronautics and Space Administration, through an Earth System Science Graduate Fellowship (Ladd) and the TOPEX extended mission (960910), and the National Science Foundation (OCE-9818920).

REFERENCES

Alexander, M. A., 1992: Midlatitude atmosphere–ocean interaction during El Niño. Part I: The North Pacific Ocean. *J. Climate,* **5,** 944–958.

——, and C. Deser, 1995: A mechanism for the recurrence of wintertime midlatitude SST anomalies. *J. Phys. Oceanogr.,* **25,** 122–137.

Bingham, F. M., 1992: Formation and spreading of subtropical mode water in the North Pacific. *J. Geophys. Res.,* **97,** 11 177–11 189.

Bjerknes, J., 1966: A possible response to the atmospheric Hadley circulation to equatorial anomalies of temperature. *Tellus,* **18,** 820–829.

Budyko, M. I., 1956: *Teplovoi Balans Zemnoi Poverkhnosti* (The Heat Balance of the Earth's Surface). Gidrometeorologicheskoi Izdatel'stvo, 255 pp. (Translated by N. A. Stepanova, U.S. Weather Bureau.)

Bunker, A. F., 1976: Computations of surface energy flux and annual air–sea interaction cycles of the North Atlantic Ocean. *Mon. Wea. Rev.,* **104,** 1122–1140.

da Silva, A. M., C. C. Young, and S. Levitus, 1994: *Atlas of Surface marine Data 1994.* Vol 1: *Algorithms and Procedures,* NOAA Atlas NESDIS 6, 51 pp.

De Miranda, A. P., B. Barnier, and W. K. Dewar, 1999: Mode waters and subduction rates in a high-resolution South Atlantic simulation. *J. Mar. Res.,* **57,** 213–244.

Esbensen, S. K., and Y. Kushnir, 1981: The heat budget of the global ocean: An atlas based on estimates from surface marine observations. Oregon State University Climate Research Institute Rep. 29, 27 pp.

Fine, R. A., R. Lukas, R. M. Bingham, M. J. Warner, and R. H. Gammon, 1994: The western equatorial Pacific: A water mass crossroads. *J. Geophys. Res.,* **99,** 25 063–25 080.

Gu, D., and S. G. H. Philander, 1997: Interdecadal climate fluctuations

that depend on exchanged between the tropics and extratropics. *Science,* **275,** 805–807.
Hallberg, R., 1995: Some aspects of the circulation in ocean basins with isopycnals intersecting sloping boundaries. Ph.D. dissertation, University of Washington, 244 pp.
Hautala, S. L., and D. H. Roemmich, 1998: Subtropical mode water in the northeast Pacific basin. *J. Geophys. Res.,* **103,** 13 055–13 066.
Hazeleger, W., and S. S. Drijfhout, 2000: Eddy subduction in a model of the subtropical gyre. *J. Phys. Oceanogr.,* **30,** 677–695.
Huang, R. X., and B. Qiu, 1994: Three-dimensional structure of the wind driven circulation in the subtropical North Pacific. *J. Phys. Oceanogr.,* **24,** 1608–1622.
Inui, T., K. Takeuchi, and K. Hanawa, 1999: A numerical investigation of the subduction process in response to an abrupt intensification of the westerlies. *J. Phys. Oceanogr.,* **29,** 1993–2015.
Isemer, H. J., and L. Hasse, 1987: *The Bunker Climate Atlas of the North Atlantic Ocean.* Vol. 2. Springer-Verlag, 252 pp.
Kraus, E. B., and J. S. Turner, 1967: A one-dimensional model of the seasonal thermocline: II. The general theory and its consequences. *Tellus,* **19,** 98–106.
Ladd, C. A., and L. Thompson, 2000: Formation mechanisms for North Pacific central and eastern subtropical mode waters. *J. Phys. Oceanogr.,* **30,** 868–887.
Ledwell, J. R., A. J. Watson, and C. S. Law, 1993: Evidence for slow mixing across the pycnocline from an open-ocean tracer-release experiment. *Nature,* **364,** 701–703.
Levitus, S., and T. P. Boyer, 1994: *World Ocean Atlas 1994.* Vol 4: *Temperature,* NOAA Atlas NESDIS 4, 117 pp.
——, R. Burgett, and T. P. Boyer, 1994: *World Ocean Atlas 1994.* Vol 3: *Salinity.* NOAA Atlas NESDIS 3, 99 pp.
Marsh, R., and A. L. New, 1996: Modeling 18° Water variability. *J. Phys. Oceanogr.,* **26,** 1059–1080.
——, A. J. G. Nurser, A. P. Megann, and A. New, 2000: Water mass transformation in the Southern Ocean of a global isopycnal coordinate GCM. *J. Phys. Oceanogr.,* **30,** 1013–1045.
Masuzawa, J., 1969: Subtropical mode water. *Deep-Sea Res.,* **16,** 463–472.
——, 1972: Water characteristics of the North Pacific Central Region. *Kuroshio—Its Physical Aspects,* H. Stommel and K. Yoshida, Eds., University of Tokyo Press, 235–352.
McCartney, M., 1982: The subtropical recirculation of mode waters. *J. Mar. Res.,* **40** (Suppl.), 427–464.
Miller, A. J., D. R. Cayan, and J. M. Oberhuber, 1994: On the reemergence of midlatitude SST anomalies. *Proc. 18th Annual Climate Diagnostic Workshop,* Boulder, CO, NOAA, 149–152.
Nakamura, H., 1996: A pycnostad on the bottom of the ventilated portion in the central subtropical North Pacific: Its distribution and formation. *J. Oceanogr.,* **52,** 171–188.
Namias, J., and R. M. Born, 1970: Temporal coherence in North Pacific sea surface temperatures. *J. Geophys. Res.,* **75,** 5952–5955.
——, and ——, 1974: Further studies of temporal coherence in North Pacific sea-surface temperature patterns. *J. Geophys. Res.,* **79,** 797–798.
Nonaka, M., S.-P. Xie, and K. Takeuchi, 2000: Equatorward spreading of a passive tracer with application to North Pacific interdecadal temperature variations. *J. Oceanogr.,* **56,** 173–183.
Nurser, A. J. G., R. Marsh, and R. G., Williams, 1999: Diagnosing water mass formation from air–sea fluxes and surface mixing. *J. Phys. Oceanogr.,* **29,** 1468–1487.
Philander, S. G. H., 1990: *El Niño, La Niña and the Southern Oscillation.* Academic Press, 293 pp.
Roden, G. I., 1970: Aspects of the mid-Pacific transition zone. *J. Geophys. Res.,* **75,** 1097–1109.
——, 1972: Temperature and salinity fronts at the boundary of the subarctic–subtropical transition zone in the western Pacific. *J. Geophys. Res.,* **77,** 7175–7187.
Schneider, N., A. J. Miller, M. A. Alexander, and C. Deser, 1999: Subduction of decadal North Pacific temperature anomalies: Observations and dynamics. *J. Phys. Oceanogr.,* **29,** 1056–1070.
Speer, K., 1997: A note on average cross-isopycnal mixing in the North Atlantic. *Deep-Sea Res.,* **44,** 1981–1990.
——, and E. Tziperman, 1992: Rates of water mass formation in the North Atlantic Ocean. *J. Phys. Oceanogr.,* **22,** 93–104.
——, H. J. Isemer, and A. Biastoch, 1995: Water mass formation from revised COADS data. *J. Phys. Oceanogr.,* **25,** 2444–2457.
——, S. Rintoul, and B. Sloyan, 1997: Subantarctic mode water formation by air–sea fluxes. *Int. WOCE Newsl.,* **29,** 29–31.
Suga, T., K. Hanawa, and Y. Toba, 1989: Subtropical mode water in the 137°E section. *J. Phys. Oceanogr.,* **19,** 1605–1618.
——, Y. Takei, and K. Hanawa, 1997: Thermostad distribution in the North Pacific subtropical gyre: The central mode water and the subtropical mode water. *J. Phys. Oceanogr.,* **27,** 140–152.
Talley, L. D., 1988: Potential vorticity distribution in the North Pacific. *J. Phys. Oceanogr.,* **18,** 89–106.
Tziperman, E., and K. Speer, 1994: A study of water mass transformation in the Mediterranean Sea: Analysis of climatological data and a simple 3-box model. *Dyn. Atmos. Oceans,* **21,** 53–82.
Walin, G., 1982: On the relation between sea-surface heat flow and thermal circulation in the ocean. *Tellus,* **34,** 187–195.
Warner, M. J., J. L. Bullister, D. P. Wisegarver, R. H. Gammon, and R. F. Weiss, 1996: Basin-wide distributions of chlorofluorocarbons CFC-11 and CFC-12 in the North Pacific: 1985–1989. *J. Geophys. Res.,* **101,** 20 525–20 542.
White, W. B., 1995: Design of a global observing system for gyre-scale upper ocean temperature variability. *Progress in Oceanography,* Vol. 36, Pergamon, 169–217.
Worthington, L. V., 1959: The 18°C water in the Sargasso Sea. *Deep-Sea Res.,* **5,** 297–305.
Yuan, X., and L. D. Talley, 1996: The subarctic frontal zone in the North Pacific: Characteristics of frontal structure from climatological data and synoptic surveys. *J. Geophys. Res.,* **101,** 16 491–16 508.
Zhang, R.-H., L. M. Rothstein, and A. J. Busalacchi, 1998: Origin of upper-ocean warming and El Niño change on decadal scales in the tropical Pacific Ocean. *Nature,* **391,** 879–883.